Towards responsive lanthanide probes for detection of reactive oxygen species

Siobhan Richardson

Towards Responsive Lanthanide Probes For Detection Of Reactive Oxygen Species

Siobhan Richardson

MSc

Department of Chemistry
Durham University

2008

Declaration

The research described in this thesis was undertaken at the Department of Chemistry of Durham University between October 2006 and September 2007. All of the work is my own; no part of it has previously been submitted for a degree at this or any other university.

Statement of Copyright

Acknowledgements

First and foremost I would like to thank my supervisor Professor David Parker, for his kind words and compassion as well as his insight into the perplexing world of chemistry. Thank you for everything.

The analytical services who were always there to help; in particular Mike Jones, Lara Turner, Alan Kenwright, Catherine Hefferman and Ian McKeag.

The members of CG27, left and leaving, thank you for your advice and suggestions.

Thank you to everyone in the department, especially certain academic staff who have helped me endlessly over the past 5 years.

Abstract

The lanthanide emissive state can be quenched by electron/charge transfer from electron rich donors, resulting in a reduction of both emissive intensity and lifetime. The quenching of luminescence by electron rich donors was further studied in an attempt to derive a feasible mechanism for the quenching process. Additional studies were performed on urate, ascorbate and series of catechols, involving ionic strength variation and extended range Stern-Volmer plots. As a result of these and further studies, a model was proposed for the quenching process; based upon the formation of a long-lived 'exciplex'.

In the proposal to synthesise complexes incorporating an intramolecular quenching moiety, two complexes have been synthesised. These complexes incorporate a tetraazatriphenylene chromophore and a methylene-protected catechol positioned trans in the cyclen ring system.

Lifetime studies on these complexes show a reduction of 35% for the Eu system (from 1.08 ms to 0.69 ms), and 70% for the Tb system (1.46 ms to 0.47 ms) with respect to analogous complexes. The difference in susceptibility of europium (III) and terbium (III) to quenching affords a promising basis for the development of a ratiometric probe.

A two-electron photoreduction was also unexpectedly observed for the Tb complex, where the bipyridyl ring undergoes irreversible reduction, confirmed by solvent deuteration and MSMS studies.

Abbreviations

Ar	Aromatic
Boc	*tert*-butoxycarbonyl
cyclen	1,4,7,10-tetraazacyclododecane
dd	doublet of doublets
DO3A	1,4,7,10-tetraazacyclododecane-1,4,7-triacetic acid
DOTA	1,4,7,10-tetraazacyclododecane-1,4,7,10-tetraacetic acid
dpqC	10,11,12,13-tetrahydrodipyrido-[3,2-a:2',3'-c]-phenazine
eT	electron transfer
ET	energy transfer
FRET	fluorescent resonance energy transfer
h	hours
HEPES	N-(2-hydroxyethyl)piperazine-N'-(2-ethanesulponic acid)
HRMS	high resolution mass spectrometry
ISC	intersystem crossing
LMCT	ligand-to-metal charge transfer
Ln	lanthanide
m	multiplet
M	mol dm^{-3}
m.p.	melting point
m/z	mass/charge
Mol	moles
MLCT	metal-to-ligand charge transfer
MRI	magnetic resonance imaging
NMR	nuclear magnetic resonance
q	quaternary
R_f	retention time
s	singlet
SAP	square anti-prism
THF	tetrahydrafuran
TSAP	twisted square anti-prism

Towards Responsive Lanthanide Probes For Detection Of Reactive Oxygen Species

1. Introduction

1.1 Reactive Oxygen Species

Reactive oxygen species are generally small highly reactive molecules of physiological and pathological importance. They can be generated by various pathways, such as the interaction of biological molecules with ionising radiation, as a by-product of cellular respiration, or be synthesised by enzymes (e.g. NADPH oxidase). Enzymes such as superoxide dismutases and catalases, and small antioxidant molecules such as ascorbic acid, uric acid and glutathione help in a cell's defence against ROS damage. It should be noted, however, that although the oxidative reactivity of ROS can cause significant damage to cell structures, they have also been attributed with important roles in chemical signalling.[1]

Molecular oxygen is typically unreactive due to the strength of the oxygen-oxygen bond and the triplet character of its ground state. For molecular oxygen to react successfully the bond strength must be weakened and/or the spin restriction removed. Therefore, when molecular oxygen is either photochemically or thermally excited to one of its singlet forms, or is reduced, its reactivity substantially increases.

$^3O_2 \rightarrow {}^1O_2$

$\downarrow e^-$

$O_2^{\bullet-} \rightarrow HO_2^{\bullet}$ (pK=4.8)

$\downarrow e^-$

$O_2^{2-} \rightarrow OH_2^- \rightarrow H_2O_2$ (pK= >14 and 11.8 respectively)

$\downarrow e^-$

$[O_2^{3-}] \rightarrow H_2O$

$\downarrow e^-$

$O^- \rightarrow HO^{\bullet}$ (pK=11.9)

$\downarrow e^-$

$O^{2-} \rightarrow H_2O$

Figure 1.1 Reduction products of molecular oxygen

Figure 1.1 illustrates the reduction products of molecular oxygen, with the most biologically important reactive oxygen species highlighted. The one electron reduction

of molecular oxygen forms superoxide, $O_2^{\bullet-}$ which is in equilibrium with its conjugate acid, the hydroperoxyl radical $HO_2^{\bullet}$. The two-electron reduction forms the peroxide ion, O_2^{2-} which is a strong base existing as hydrogen peroxide at physiological pH. These species have enhanced reactivity with respect to oxygen, as the additional electrons occupy antibonding orbitals thus removing bond strength as well as the spin restriction. Another important oxygen species is the hydroxyl radical, which is highly reactive, being produced mainly from side reactions of other ROS, such as the reaction of metal ions with H_2O_2 or the UV-induced homolytic fission of H_2O_2.[2]

Each ROS has unique physiological activity, which as well as being peculiar to the molecule is also dependent on the environmental conditions in which it is placed, such as temperature, pH, other ROS and molecules present, and concentration. Table 1.1 states the reduction potentials for some biologically important and relevant molecules, although the factors listed above must be considered as they may profoundly influence these values. The reduction potentials show that ROS are potentially able to oxidise urate and ascorbate, and may thus be reduced themselves.

	Couple	Standard Reduction Potential (V)
Most Reducing	$Ascorbate^{\bullet-}$, H^+ / $Ascorbate^-$	0.30
	H_2O_2, H^+ / H_2O, $OH^{\bullet}$	0.32
	$HU^{\bullet-}$, H^+ / UH_2^- (Urate)	0.59
	$O_2^{\bullet-}$, $2H^+$ / H_2O_2	0.94
	$HO_2^{\bullet}$, H^+ / H_2O_2	1.06
Most Oxidising	$OH^{\bullet}$, H^+ / H_2O	2.31

Table 1.1 Biologically important standard reduction potentials. For each couple the oxidised species is on the left and reduced on the right. Measurements are corrected to pH 7 and are at 298K. Singlet oxygen is an excited state species lying 96 kJmol^{-1} higher in energy than the ground state (ca. +1V).

The detection and quantification of ROS has been the subject of intensive research due to their importance in both biological damage and function. Recently, reviews examining and challenging the current work in this area have been published. It is the restrictions and inherent limitations in this work that render it difficult to establish a successful detection method for ROS (see Section 1.1.5; pg. 11).[3 4]

Spectroscopic probes are the most widely used technique for the examination of reactive oxygen species, encompassing methods such as electron spin resonance, spectrophotometry, fluorescence and luminescence. Fluorescence and luminescence are being increasingly used for *in vivo* systems, as they are able to provide spatial and temporal information on target biomolecules, thus enabling interpretation of *in cellulo* activity. Selectivity is a major concern in the development of ROS specific probes. Each ROS has its own unique physiological behaviour/activity therefore distinguishing between them should be possible due to the difference in rate and reactivity. Individual ROS detection and monitoring will ultimately enable an understanding of physiological mechanisms and behaviour.

Derivatives of fluorescein are extensively used in this area of study due to their high quantum yield of fluorescence under aqueous conditions, their long excitation wavelength (thus avoiding coexcitation of common biomolecules) and reasonably high extinction coefficient. Therefore, fluorescein has been widely used as a fluorophore for the labelling and detection of biomolecules.[5]

A traditionally used probe is 2',7'-dichlorodihydrofluorescein (DCFH), which was originally pioneered by Keston and Brandt as a fluorescent probe for hydrogen peroxide.[6] Development of this probe has led to a family of dihydrofluorescein compounds of varying structure and selectivity. Figure 1.2 illustrates the mechanism by which DCFH-DA enters cells and is oxidised to yield fluorescent DCF.

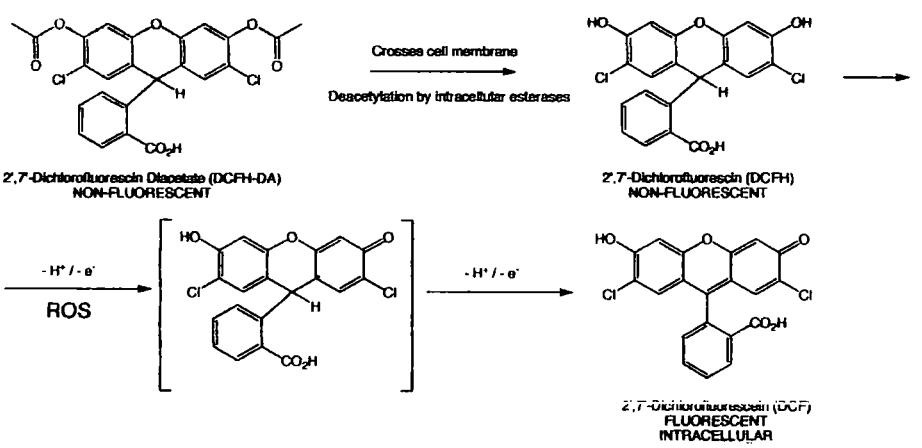

Figure 1.2 The process of DCFH-DA entry into cells via hydrolysis to produce non-fluorescent DCFH followed by oxidation by ROS to yield the fluorescent DCF.

λ_{ex}=488 nm, λ_{em}=525 nm.

Over the years following the proposal and use of this probe there has been much debate as to the nature of the ROS responsible for the oxidation of DCFH.[7] It has been found that there are several reactive species that are responsible for oxidising DCFH; therefore results have to be interpreted critically, especially when trying to relate oxidation to a particular reactive species. It is this lack of selectivity which means they are unsuitable for the detection of individual ROS, but are argued to be 'suitable' for detecting total oxidative activity in living cells or tissue. This point is debatable, due to the general problems that arise from the *in vivo* detection of ROS (see Section 1.1.5; pg. 11). Coupled with the problem of selectivity, these probes are also photosensitive. Autoxidation of these probes by the excitation light even in the absence of ROS, results in large background fluorescence; this makes quantification of fluorescence intensity difficult. Even if a correction is made, other influential factors on this autoxidation need to be considered. Even though these probes are dated and flawed the extensive studies that have been performed on DCFH and its family have led to important information on problems arising in the development and application of ROS probes.[3]

1.1.1 Singlet Oxygen Probes

Along with hydrogen peroxide, singlet oxygen is one of the most extensively studied ROS due to its longer lifetime with respect to other reactive oxygen species. There are two forms of singlet oxygen, but the $^1\Sigma_g$ form rapidly decays to $^1\Delta_g$, so the latter is the only biologically significant form. Singlet oxygen can transfer its excitation energy to proximate solvent molecules. Therefore, its lifetime is dependent upon the conditions; the lifetime in water is typically 4 μs. Other than energy transfer to proximate molecules, it is also chemically reactive forming dioxetanes[8] or endoperoxides; it is the formation of endoperoxides by a Diels-Alder reaction that is most frequently utilised for the detection of singlet oxygen.

Work by Nagano yielded the DPAX and DMAX (Figure 1.3) fluorescent probes, which are examples of fluorescein derivatives that are more selective in their application than the DCFH family. Instead of being facilitated by electron transfer, which in the case of the DCFH family led to lack of selectivity, this reaction is driven by the formation of an endoperoxide across the ring system.[9]

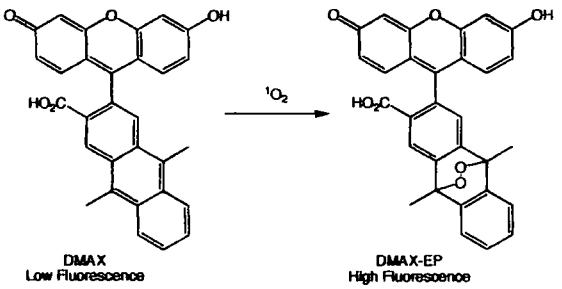

Figure 1.3 Formation of endoperoxide across DMAX ring due to reaction with singlet oxygen. λ_{ex}*~492 nm,* λ_{em}*~515 nm.*

DMAX is more sensitive than its precursor DPAX. The fluorescent properties of these molecules arise from the photoinduced electron transfer from the benzoic acid moiety to the xanthene ring, and by chemically altering the level of the HOMO via substitution, the fluorescence properties were modified. The addition of a dimethylanthracene system to fluorescein resulted in the non-fluorescent species DMAX that reacts readily with singlet oxygen to yield the highly fluorescent DMAX-1-EP. This modification gave a higher quantum yield difference but similar excitation and emission characteristics. The reaction rate of DMAX was higher (x31) with improved sensitivity (x53) for singlet oxygen. The compound is also more hydrophilic and thus more biologically suitable. Studies with various ROS showed DMAX to be highly selective for singlet oxygen, not reacting with other species to any extent. Although this is an example of a chemoselective fluorescent probe, the Stokes' shift is relatively small. Thus, co-excitation should be considered; this is an issue present in many of the ROS probes. Also, these probes are not suitable in all conditions, as endoperoxides are non-fluorescent at low pH.

Yuan presented a luminescent europium complex that was also based upon the principle of a cycloaddition reaction with singlet oxygen (Figure 1.4).[10] The rate constants for these probes were higher than those of other aromatic compounds in [2+4] cycloadditions. This was attributed to the conjugation of the fluorophore, TTA-Eu^{3+} with the anthracene framework, with the Lewis acidic lanthanide centre serving to enhance the reactivity of the diene component in the pericyclic reaction.

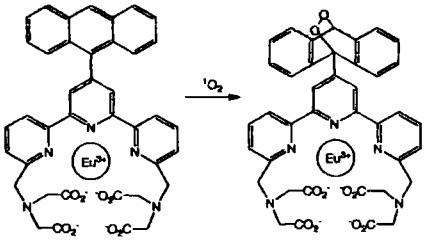

Figure 1.4 Reaction of ATTA-Eu^{3+} with $^1O_2$ to form EP-ATTA-Eu^{3+}.
λ_{ex}=335 nm, λ_{em}=615 nm

The quantum yield for lanthanide emission of the complex increases 17 fold following cycloaddition, as the anthracene moiety no longer quenches luminescence. The complex was shown to have no bound water molecules via lifetime measurements, showing that the change in fluorescence is not due to water exchange. The complex is stable over the pH range 3 to 10 and therefore is useful under various physiological conditions. The lanthanide centre also provides a large Stokes shift, which helps to avoid co-excitation. A good linear response was observed between $^1O_2$ concentration and fluorescence, with a detection limit of 2.8 nM and comparatively high sensitivity for $^1O_2$ over other ROS. Further work within the group has led to the introduction of a new probe, MTTA-Eu^{3+}, which has an additional methyl group on the anthryl moiety at the site of epoxidation. The reaction rate for this probe is faster than that of ATTA-Eu^{3+} therefore providing better detection of the short-lived $^1O_2$ species. The detection limit for this probe is 3.8 nM, which is similar to that of the previously reported complex. Furthermore, the complex was shown to enter cells and allowed time-dependent $^1O_2$ generation to be monitored.[11] Although ATTA-Eu^{3+} and MTTA-Eu^{3+} are novel ROS probes, as the cycloaddition is irreversible the complex will be consumed during the reaction. This irreversibility results in emissive complex with limited applications. For example, if the local concentration of ROS is changing with time, the complex cannot give a measure of this, as it basically acts as an 'off/on' switch.

1.1.2 Hydrogen Peroxide Probes

Hydrogen peroxide is the least reactive of the ROS; although it has a major role in the production of other ROS. It has been extensively studied and probes include various families such as the sulphonyls, boranes, phosphines[12] and europium complexes.

Wolfbeis has proposed the use of a europium complex for the detection of hydrogen peroxide. This work is of limited value. Firstly, the ligand only forms a very weakly bound complex with Eu (III), therefore a continual exchange will be occurring in solution and the structure cannot be defined. The response of the complex is also highly pH dependent with the luminescence intensity dropping to 15% of its maximum value at pH 8 and 6% at pH 6. The decay profiles are also said to exhibit more than one component, and no studies are performed with other ROS. Although a detection limit of 1.8 μM is quoted, this number is invalid due to the number of events that could be taking place in solution.[13]

Maeda has adopted a deprotection approach to fluorescence, arguing that non-oxidative systems are more appropriate for the detection of ROS as they are more selective and less subject to the complicated oxidative conditions found in biological systems. The design of pentafluorobenzenesulfonyl fluoresceins was based on the idea that sulfonates are more stable to hydrolysis than esters and thus more selective; the pentafluorobenzene ring increases the reactivity of sulfonates to hydrogen peroxide (Figure 1.5).[14]

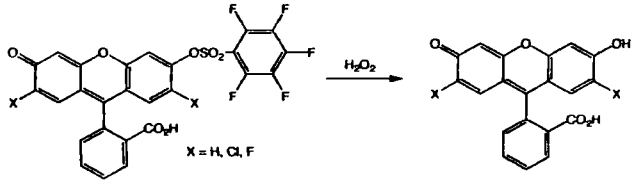

Figure 1.5 Pentafluorobenzenesulfonyl fluorescein probes.
λ_{ex}=492 nm, λ_{em}=525 nm.

Although these probes did demonstrate enhanced selectivity with respect to DCFH they did show reactivity towards other ROS and other reactive species such as NO•. The detection limit was quoted to be up to 4.6 pmol but this value is highly dependent on the conditions; as temperature and pH significantly affected the detection limit, rate of reaction, fluorescence intensity and the rate of decomposition. As observed previously, this probe is also consumed due to the irreversibility of the reaction. The quantum yield difference was also very small between the non-fluorescent and fluorescent probe. Therefore, accuracy may be an issue when errors are considerably large.

Chang also used deprotection methodology for detection of hydrogen peroxide, where arylboranes were converted into phenols.[15] The initial probe developed was peroxyfluor-1, PF1, and further work led to a trio of probes, including peroxyresorufin-1, PR1 and peroxyxanthone-1, PX1 (Figure 1.6).[16]

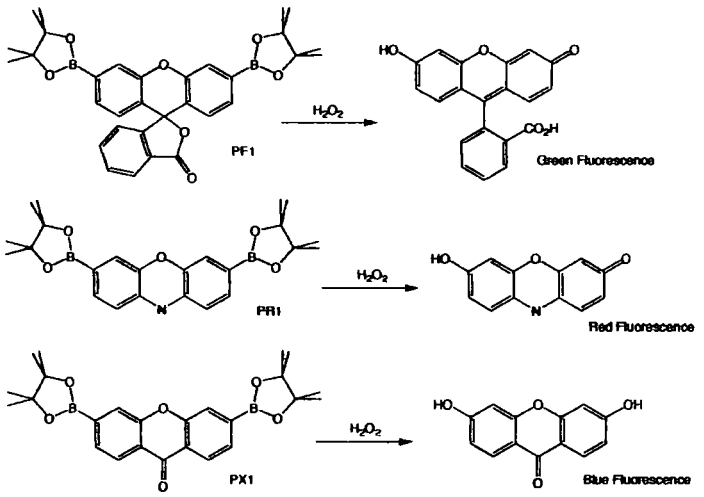

Figure 1.6 Peroxyfluor-1 PF1, Peroxyresorufin-1 PR1 and Peroxyxanthone-1 PX1. PF1:λ_{ex}=450 nm, λ_{em}=520 nm, PR1:λ_{ex}=530 nm, λ_{em}=590 nm, PX1:λ_{ex}=350 nm, λ_{em}=440 nm.

These probes all function via a boronate deprotection mechanism driven by H_2O_2, resulting in fluorescence spanning the ultraviolet through to the visible. Each of these probes has an enhanced sensitivity with respect to other ROS, which is proposed to be due to the detection mechanism being based on deprotection rather than oxidation to provide an optical response. It should be noted that the selectivity varies slightly for each probe. The red probe is proposed to be the most useful, as red emission is of lower energy thus minimising cellular absorbance, scattering and autofluorescence. The PR1 and PF1 compounds possess a 5- to 500- improvement in the H_2O_2 dynamic range, with respect to the previously reported probes. The fluorescence change on H_2O_2 recognition is >1000 fold, with respect to the integrated emission, and as such will minimise error. DCFH probes show a comparable dynamic range to this series but are not as selective in their reactions with ROS. A calibration plot for PF1 shows a linear correlation between the amount of H_2O_2 added and the fluorescence response after 15 minutes. The detection limit is stated to detect H_2O_2 reliably down to concentrations of 100-200 nM *in vitro*. All three probes are cell permeable and have been demonstrated to function within cells detecting H_2O_2 within micromolar concentrations, with two-photon excitation being used for PX1, and confocal microscopy for observation.

Recently PF1 has been developed as a ratiometric fluorescence probe incorporating FRET (Figure 1.7).[17]

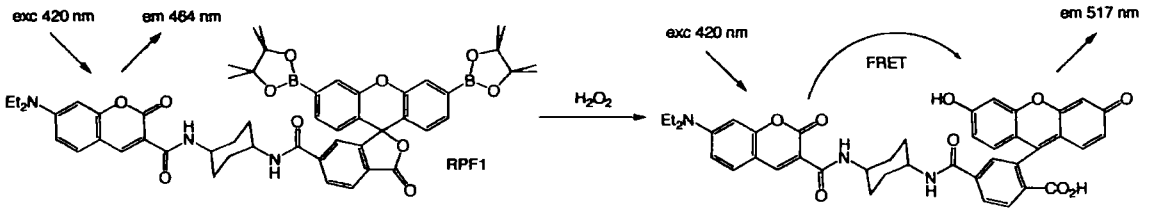

Figure 1.7 RPF1 is deprotected by H_2O_2 and FRET enables ratiometric fluorescence

Fluorescence resonance energy transfer (FRET) between a coumarin donor and rigidly linked PF1 is suppressed in the boronate protected form but as deprotection occurs on reaction with H_2O_2 the fluoroscein acceptor shows a strong absorption in the region of the blue coumarin emission spectrum resulting in increased green fluorescence by FRET. Changes in the ratio of the blue fluorescence (464 nm) to the green fluorescence (517 nm) give a ratiometric measure of H_2O_2 concentration. Although this is a novel idea especially when considering biological problems such as probe concentration/environment, sample thickness, emission collection efficiency, and variation in excitation intensity, this probe is a lot less sensitive to H_2O_2 than the previously reported PF1; PF1 was incredibly discriminate being 100-500 times more selective for H_2O_2 over other ROS. The only major competing reactive species was nitric oxide gas, but the probe was still 6 times more selective, whereas RPF1 is only 3-8 times more selective for H_2O_2 than for other ROS and RNS.

1.1.3 Superoxide Probes

An example of a superoxide probe has been developed by Maeda (Figure 1.8). This probe is similar to that designed for the detection of hydrogen peroxide but with some structural modifications. The detection of $O_2^{\bullet-}$ is based upon the deprotection of a bis-sulfonylated fluorescein, which when substituted with nitro groups shows enhanced reactivity towards $O_2^{\bullet-}$ but not H_2O_2[18]

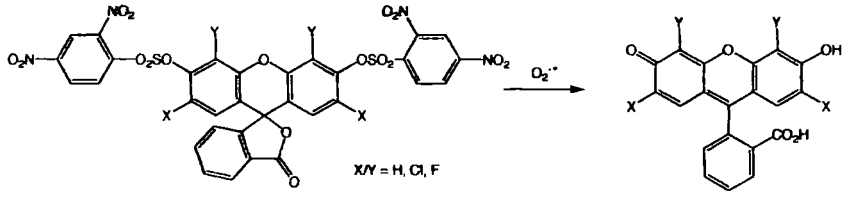

Figure 1.8 Bis(2,4-dinitrobenzenesulfonyl) fluorescein probes.

Although these probes have a detection limit of 1.0 pmol and exhibit a linear response, they have also been shown to have enhanced reactivity towards thiols and reductases, as a result of the dinitrobenzene sulphonyl functionality.

Scaiano has recently developed a probe for peroxyl radical detection, $RO_2^{\bullet}$. The compound NBFhd contains a fluorescent moiety, N-methyl-4-amino-7-nitrobenzenefurazan (NBF), linked to a phenolic structure that acts as both a quencher and hydrogen donor (Figure 1.9).[19]

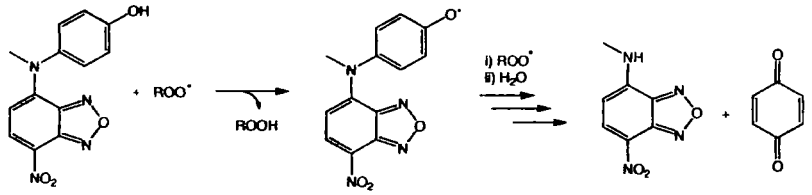

Figure 1.9 Proposed reaction mechanism of NBFhd with peroxyl radicals.
λ_{ex}=468 nm, λ_{em}=540 nm.

The phenol quenches the fluorescence of the excited NBF via electron transfer. Interaction with peroxyl radicals results in hydrogen abstraction from the phenolic ring and then a second peroxyl radical results in the dissociation of 1,4-benzoquinone yielding the fluorescent NBF (although the quantum yield in water is only 2.6%). A linear response was established between fluorescence intensity and time, although after approximately 2 hours the fluorescence begins to decrease. This is thought to be a result of peroxyl radical attack on NBF. It was noted that only 15-20% of NBF was released from the reaction with the peroxyl radical, owing to the side reactions that were occurring after the primary hydrogen abstraction by the peroxyl radical. The intermediate NBFhd radical can couple with other radical species forming side products. These side reactions cause problems with sensitivity, as the reaction will be highly dependent on the conditions of reaction with various competing rates. The probe

is also not very selective; although it was shown not to react with H_2O_2, it does react with both hydroxyl radicals $OH^{\bullet}$ and superoxide $O_2^{\bullet-}$. Such a reactivity profile is to be expected, considering the nature of the reaction, as the probe is likely to react with most radical species.

1.1.4 Hydroxyl Radical Probes

Hydroxyl radicals are highly reactive and therefore their detection is difficult to measure specifically or selectively. Methods of detection often resemble[20] those mentioned above in the case of the Scaiano probe, where a group such as 1,4-benzoquinone is released promoting fluorescence of the other moiety. As these reactions occur in various stages there is time for coupling of radicals, chain reactions and many competing processes to interfere with measurements.

Nagano introduced the HPF and APF probes, which resist autooxidation and are highly selective. Once again, these probes are based upon fluorescein (Figure 1.10). They fluoresce on reaction with $OH^{\bullet}$ and $ONOO^-$ but are unresponsive to $^1O_2$, $O_2^{\bullet-}$, H_2O_2 and $RO_2^{\bullet}$.[21]

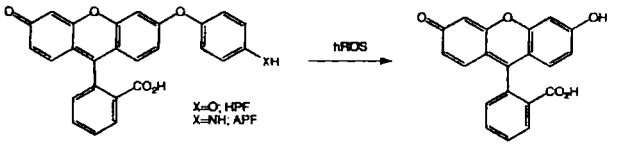

Figure 1.10 – Reaction of HPF and APF with highly ROS.
λ_{ex}=490 nm, λ_{em}=515 nm.

One interesting probe was proposed by Imato, which involves a ratiometric probe for hydroxyl radicals involving FRET. The fluorescence as a result of FRET decreases with increasing $OH^{\bullet}$ and the fluorescence of the absorbing moiety increases, thus providing a selective measure of $OH^{\bullet}$ concentrations lower than 100 μM.[22]

1.1.5 Probe and Detection Limitations

The limitations of currently available probes are extensive, and each probe suffers from these to a greater or lesser degree. Problems include the chemical instability of the probe, instability of the product of reaction, hydrolysis of precursors of probe, absence

of specificity for a given ROS, oxidation/reduction of the probe by other species, generation of ROS due to system disruption, location specificity, problems with artefacts, and relative proportionality to ROS production. This is not even considering basic chemical problems. These include a probe's insolubility that may often require use of an organic cosolvent, membrane permeability, excitation profile, co-excitation and problems with interference from autofluorescence.[3]

Relatively few probes demonstrate ratiometric methodology. In practice this is what is required of a ROS probe. As well as the issues listed above, others must be considered when measuring ROS. Firstly, a valid appropriate probe must be presented. The fluorescence intensity of a probe is generally very susceptible to the environment, where the presence of other species as well as variations in pH, temperature, and probe concentration can all potentially cause fluorescence fluctuations; and these issues must be confronted and not avoided. Even in cases where probes appear to be stable and consistent with respect to their photophysical chemistry, when they enter a cell very different results may be observed.[23] Therefore, ratiometric probes, which incorporate the facility of 'on-off or off-on' switching, are necessary.

1.2 Lanthanide Complex Chemistry

1.2.1 Lanthanide Chemistry

Increasing interest in the luminescent properties of lanthanide complexes over the last 20 years has resulted in the discovery and rapid development of their application as biological contrast agents and luminescent probes in the detection and monitoring of chemical species.[24]

The distinctive tendency of the lanthanides to form the +3 oxidation state is due to the high sensitivity of the valence *4f* electrons to the core nuclear charge; where the formation of Ln^{3+} enables the *4f* electrons to participate in chemical reactivity. Lanthanide (III) ions have highly contracted *4f* orbitals; and due to shielding from the *5s* and *5p* orbital electrons, *4f* electrons are not readily involved in bonding and the chemical properties of the series are highly uniform. As a consequence of this contraction, the *4f* electrons have no significant stereochemical influence on ligand

coordination. Hence, complexation is primarily electrostatic, and coordination number is dependent on ligand steric effects about the metal centre. The coordination number, which ranges from 9-6, decreases across the series due to the lanthanide contraction.[25 26 27]

Lanthanides are used in luminescent complexes due to the extensive excited state chemistry which can occur when the metal is coordinated to a variety of organic ligands, which themselves may have interesting excited state chemistry. The long lived emission of lanthanide complexes allows time resolved detection to be employed. This is essential for use in cells, as it provides a distinction between the sensor and background emission, as the background emission will have decayed to negligible levels and the lanthanide emission can be monitored with no interference. The lowest energy excited states of several lanthanide ions have long natural radiative lifetimes of between 0.1 and 10ms. Luminescent probes are usually centred on either europium or terbium, which emit red and green light respectively.[28]

The absorption and emission spectra of the lanthanide (III) ions may be interpreted in terms of energy levels defined by the Russell–Saunders coupling scheme, where the ordering of these energy levels is predicted by Hund's Rules. The energy gap between neighbouring terms is usually 5000-10000 cm^{-1}, and 1000 cm^{-1} between the J levels of each term. Rapid internal conversion occurs to the lowest lying J state of the first excited state of the lanthanide (III) ion. Emission therefore typically occurs from one electronic state and thus a series of bands to multiple J levels are formed on emission to the ground state (Figure 1.11).[24 28 29]

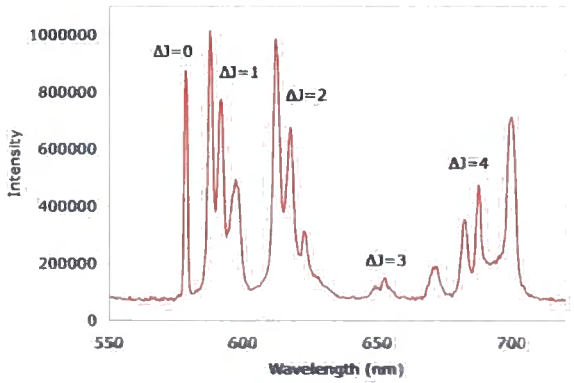

Figure 1.11 Emission spectrum of luminescent lanthanide complex, EuDO3AAzaH

The emissive properties of the Ln^{3+} ions are influenced by the contracted nature of the 4*f* orbitals which has several consequences: transitions between energetic states are independent of ligand or phase (the lack of metal-ligand interaction results in minimal ligand field splitting of ~100 cm^{-1}); also metal-ligand distances have little effect on the excited state energies producing sharp bands and distinct absorption. Finally, as *f-f* (and *d-d*) transitions are *Laporte forbidden* (as a result of the symmetry selection rule), the transitions are weak. The transition metals have expanded *d* orbitals, which allow for transitions to be partially permitted as a result of vibrational mode mixing with the coordinating ligands. Additionally, as the lanthanides lack significant interaction with the coordinating ligands the transitions remain weak; a consequence is that the molar extinction coefficients are small (typically $\varepsilon = 0.5\text{-}3$ $dm^3mol^{-1}cm^{-1}$).[25 30]

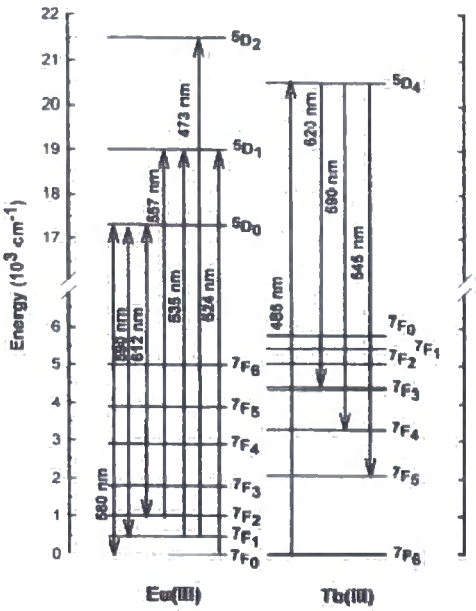

Figure 1.12 Transition diagram for Eu^{3+} and Tb^{3+}

For Eu^{3+} complexes the dominant transitions are $^5D_0 \rightarrow {}^7F_{1,2}$ (Figure 1.12). The $^5D_0 \rightarrow {}^7F_1$ (590 nm) transition is a magnetic dipole emission, independent of the coordination sphere, whereas the $^5D_0 \rightarrow {}^7F_2$ (612 nm) transition is a hypersensitive induced electric dipole emission that is extremely sensitive to the symmetry of the coordination sphere. Richardson and co-workers established[31], in a centrosymmetric environment, that the $^5D_0 \rightarrow {}^7F_1$ ($\Delta J=1$) transition is dominant, whereas distortion of symmetry around the metal results in the $^5D_0 \rightarrow {}^7F_2$ ($\Delta J=2$) transition becoming dominant due to the intensity enhancement of electric dipole transitions. Thus, the

relative intensities of the $^5D_0 \rightarrow {}^7F_1$ and $^5D_0 \rightarrow {}^7F_2$ emission in europium (III) complexes can reveal the varying symmetry about the metal ion. The intensity of the hypersensitive $\Delta J=2$ and $\Delta J=4$ (690 nm) bands of the europium emission spectra are sensitive to the ligand field, especially the nature and polarisability of the axial donor. Therefore, it can be considered a 'fingerprint' of the Eu^{3+} coordination environment. The $^5D_0 \rightarrow {}^7F_0$ (580 nm) transition is a weak ($\Delta J=0 \rightarrow \Delta J=0$ is forbidden) induced electric dipole transition, but as the states are non-degenerate the number of emission bands observed can be used to probe the number of Eu^{3+} chemical environments.[27 32 33]

For Tb^{3+} complexes, the $^5D_4 \rightarrow {}^7F_5$ (545 nm) is the dominant transition, which is also hypersensitive but not as susceptible to changes in the environment as the dominant $^5D_0 \rightarrow {}^7F_2$ in Eu^{3+} complexes. There is difficulty in establishing the symmetry of the metal ion as the large number of J-values for the levels causes splitting, thus the fine structure cannot be fully resolved.[24 33]

1.2.2 Sensitised Emission

Population of lanthanide (III) excited states is difficult to achieve via the direct absorption of light as a result of low molar absorption coefficients. Alternatively, first described by Weissman,[34] a chromophore possessing a suitable absorption band can be positioned in close proximity to the lanthanide ion. This 'antenna' will absorb strongly from conventional light sources, and facilitate the energy transfer of the absorbed light from its excited state to the lanthanide emissive state (Figure 1.13). If the chromophore has a high extinction coefficient and energy transfer to the lanthanide (III) ion is successful, then the molar absorption coefficient of the metal ion is effectively increased which can lead to intense luminescence following excitation.

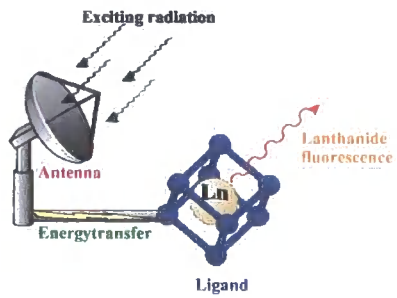

Figure 1.13 Sensitised emission

Absorption of energy by the chromophore results in promotion to a higher energy singlet state, which can then decay by fluorescence or undergo intersystem crossing to a triplet state of similar energy. This triplet state can decay by three processes: sensitiser phosphorescence, intersystem crossing back to the singlet band, or, if the triplet state is of comparable energy to the lanthanide emissive state, the energy can be transferred to the lanthanide. Absorption of light by lanthanide (III) ions results in the population of the excited state, which is of a different multiplicity to the ground state. Releasing the deactivating photon to regenerate the ground state is spin forbidden, resulting in a phosphorescence process involving the storage of energy in a reservoir; consequently the energy is then slowly released and the emission gives rise to luminescence (Figure 1.14).[28 30]

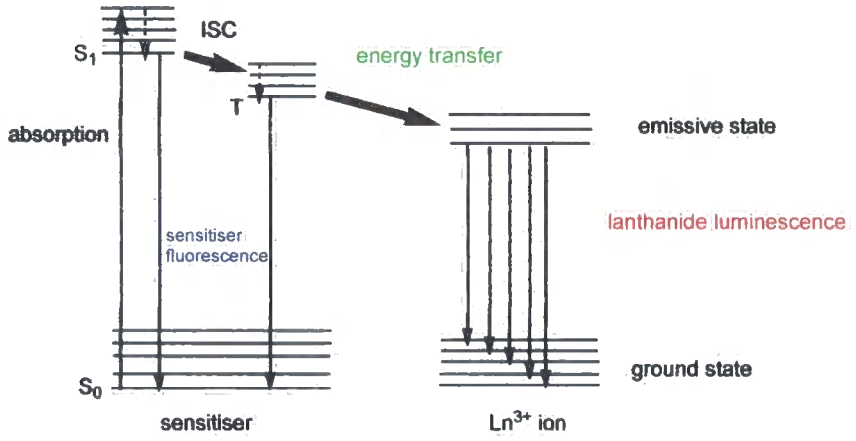

Figure 1.14 Sensitised emission energy transfer schematic

Development of chromophores has shown some common requirements for successful energy transfer to lanthanide (III) ions. The most commonly studied emissive lanthanide ions are Eu and Tb, possessing excited $^5D_0$ and $^5D_4$ states of 17240 cm^{-1} and 20400 cm^{-1} respectively. The chromophore therefore, needs to have a singlet state of comparable energy, and a small singlet-triplet energy gap. To allow both Eu and Tb excitation, it is preferable to have a triplet excited state in the range 22500-25000 cm^{-1}. The triplet excited state energy of the chromophore must be at least 1700 cm^{-1} above that of the lanthanide excited state, as if the energy difference is less than 1500 cm^{-1} thermally activated back transfer competes with the luminescence process, resulting in repopulation of the triplet state. Similarly if the energy gap is too large then the energy transfer is less efficient – a balance is therefore required to ensure effective transfer.[30]

The reduction of Eu^{3+} (f^8) to Eu^{2+} (f^7) is easily facilitated, therefore europium (III) is susceptible to reduction by the chromophore; this photoinduced electron transfer results in the formation of the radical cation and Eu^{2+} limiting the overall quantum yield. Reduction of the europium (III) ion can be prevented if the oxidation potential of the chromophore is increased.[35]

The electronic energy transfer between the lanthanide (III) ion and sensitiser can be ascribed to either the Förster or Dexter mechanism, which both describe non-radiative electronic energy transfers. The Förster mechanism involves a through space dipole-dipole interaction primarily dependent on the overlap of the emission spectrum of the donor (sensitiser), and absorption spectrum of the acceptor (Ln^{3+}). This can be expressed as the rate of energy transfer, k_{ET}, as a function of the separation, r, between the two species, where $k_{ET} \propto 1/r^6$.[36] The Dexter mechanism involves electron exchange between the two species, which is dependent on electronic orbital overlap as well as spectral overlap. The exchange of electrons from the excited sensitiser to the lanthanide and vice versa occurs over distances larger than van der Waals interactions, diminishing rapidly at distances greater than 5Å; with rate of energy transfer decreasing exponentially with increasing separation, due to decreasing orbital overlap.[37] Ultimately both mechanisms rely upon intramolecular separation; therefore, rate and efficiency of electronic energy transfer is greatly enhanced if the distance is minimised.[38]

1.2.3 The Complex – Issues in Practical Application

Issues relating to the application of these complexes are: an appropriate excitation wavelength; the overall quantum yield; the stability/toxicity of the complex; and the potential quenching routes of energy transfer (see Section 1.2.6; pg. 21).

The chromophore must have an appropriate excitation wavelength, as well as a reasonable molar absorption coefficient, with a range reflecting the application. Wavelengths between 337-420 nm are most suitable for *in cellulo* applications as they avoid the co-excitation of common biomolecules (proteins, aromatic amino acids, nucleic acids) and are appropriate for the triplet energy requirement.[39]

The product of three photophysical steps defines the overall quantum yield:

$$\phi_{tot} = \phi_A \eta_{ET} \phi_{em}$$

$$\phi_{em} = k_0 \tau_{obs}$$

$$\phi_{tot} = \phi_A \eta_{ET} k_0 \tau_{obs}$$

Namely, the quantum yield of the intersystem crossing to form the intermediate aryl triplet state and the energy transfer between the triplet state and the lanthanide (with regards to its respective rate and efficiency, η_{ET}). The energy transfer is most efficient when the chromophore and lanthanide are in close proximity, there is a small but balanced energy gap, and no competing back energy transfer. Finally, the product of the observed luminescence lifetime and the natural radiative rate constant (in the absence of deactivating processes) gives the emissive quantum yield of the lanthanide ion.[40]

The probe must resist premature decomplexation or chemical degradation therefore it must be kinetically stable with respect to cellular conditions. Hence, it must be stable in the pH range 3-10 preferably in a 1:1 metal:ligand complex; this is achieved with a high coordinating ligand shielding the lanthanide ion from quenching – this is a 7-9 coordinating ligand with ideally at least one donor atom from the chromophore.[30]

1.2.4 Ligand and Chromophore Design

There have been a variety of ligands and chromophores explored for the use of Eu^{3+} and Tb^{3+} as luminescent probes. The complexing ligand must be suited to its application. For *in cellulo* applications, analogies can be drawn with MRI gadolinium complexes used *in vivo*.[27] Most importantly; the complex must be kinetically and thermodynamically stable in solution, preferably over a wide pH range. Highly contracted 4*f* orbitals (low polarisability), and the high positive charge (+3) of lanthanide (III) ion, result in ionic bonding interactions with a preference for hard donors such as oxygen and nitrogen. Neutral donors such as the oxygen donors of amides coordinate strongly due to the large ground state dipole moment, and charged oxygen donors present in carboxylates and phosphinates. The hydration number of Eu^{3+} and Tb^{3+} is typically 8 or 9, therefore the coordinating ligand should preferably have this number of donor atoms to obtain a solvent free complex.[35] As the complexes are to be used in an aqueous environment, macrocyclic ligands are most appropriate as the 'chelate' and 'macrocyclic effect' result in high binding constants so that hydration is

minimised in solution, as well as avoiding biomolecule ligation – thus a complementary ligand with a high degree of preorganisation will provide a suitably stable complex.[41] A variety of ligands have been developed for these purposes eg. β-diketonates, cyclen derivatives, cryptates, EDTA and DTPA derivatives, calix [4] arenes, and *m*-terphenyl-based ligand systems.[42]

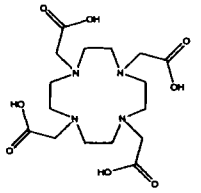

Figure 1.15 DOTA ligand

The 1,4,7,10-tetraazacyclododecane (cyclen) macrocycle coordinates to the lanthanide via 4 nitrogen donors and the incorporation of arms to the donor atoms additionally stabilises the complex, resulting in a cage-like ligand. 1,4,7,10-Tetraazacyclododecane-1,4,7,10-tetraacetic acid, DOTA (Figure 1.15), is an analogue of the cyclen ring with 4 carboxylate arms attached via the nitrogen atoms. Related ligands involve phosphonate, phosphinate or amide groups as the coordinating arms. The complex can be anionic, cationic or neutral depending on the nature of these arms. The caging prevents dissociation and quenching via water molecules, improving quantum yield and therefore luminescence. Attachment of the sensitiser to the cyclen ring (substituting an arm) minimises the metal and chromophore separation and promotes energy transfer. Typically, 9 coordinate complexes exist as isomeric species in solution, defined by torsion angles and adopting structures based upon either a square antiprism (SAP) or twisted square antiprism (TSAP) geometries. A number of articles discuss the geometry about the metal centre, water coordination and exchange dynamics.[32 33 43 44]

As mentioned previously, requirements for a suitable chromophore are; a reasonably high molar absorption coefficient in the range of 337-420 nm, an efficient intersystem crossing step, a triplet level above 22,500 cm^{-1} and preferably at least one donor atom on the sensitiser to minimise separation from the lanthanide.

Sensitisers of particular interest and development over the last decade have been based upon tetraazatriphenylene and aryl ketone derivatives.

Tetraazatriphenylene sensitisers (Figure 1.16) have been under development for some time,[45] as they possess a high excitation wavelength, and a small singlet-triplet energy gap providing an efficient intersystem crossing step and thus producing high quantum yields. They also have the ability to coordinate in a bidentate manner to the lanthanide centre. Meticulous work within the Durham group has studied these complexes, incorporating various tetraazatriphenylene sensitisers, in cellular environments and as DNA probes.[46]

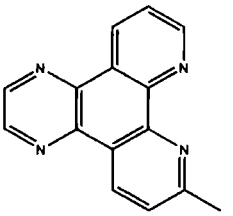

Figure 1.16 Tetraazatriphenylene sensitiser (λ_{ex} ~ 340nm), (Triplet energy ~ 23500 cm^{-1})

Aryl ketones have been extensively studied as they form versatile structures that are amenable to systematic variation and hence resolving some of the problems that are faced in the development of luminescent probes. Chromophores such as substituted acridones,[47] benzophenones,[48] acetophenones,[49] and azaxanthones/azathioxanthones[50] (Figure 1.17) have been developed, all possessing various photophysical properties depending on the nature of the structure. The Durham group has also applied azaxanthone and azathioxanthone complexes to *in cellulo* environments, where they show differing localisation profiles depending on the nature of the ligand structure.[51]

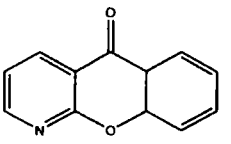

Figure 1.17 Azaxanthone sensitiser (λ_{ex}=333nm), (Triplet energy ~ 24800 cm^{-1})

1.2.5 Cellular Application

The use of time-resolved homogeneous assays in analytical biochemistry and high throughput screening has been highly successful; so, the development of suitable luminescent probes for *in cellulo* applications is promising. It is hoped that eventually this can be extended to *in vivo* applications. It is known that light in the range of 710-820nm penetrates skin and tissue most effectively, thus near-IR emitting luminescent

probes may be more appropriate, unless Eu^{3+} and Tb^{3+} luminescent probes can integrate two-photon excitation. Typical types of probes are either for the detection or monitoring of chemical species. Detection involves tracking or tagging, and monitoring is concerned with responsive systems, where the properties vary as a function of local concentration of a target intracellular analyte. As well as being cell permeable, the emissive probe must also show a distinctive compartmentalisation profile so that it localises in a given organelle. Various lanthanide complexes incorporating a range of sensitisers, coordinating arms and overall complex charge have been applied to cellular environments and show a range of localisation profiles and luminescence. The variation of luminescence when the complexes are applied to cells is a result of various forms of *in cellulo* quenching, particularly by photoinduced electron transfer, so it is important to consider the role of such electron rich species i.e., ascorbate and urate.[23 39 52]

1.2.6 Quenching Processes

Quenching at every stage of the energy transfer processes must be considered as it limits the overall emission quantum yield (Figure 1.18).

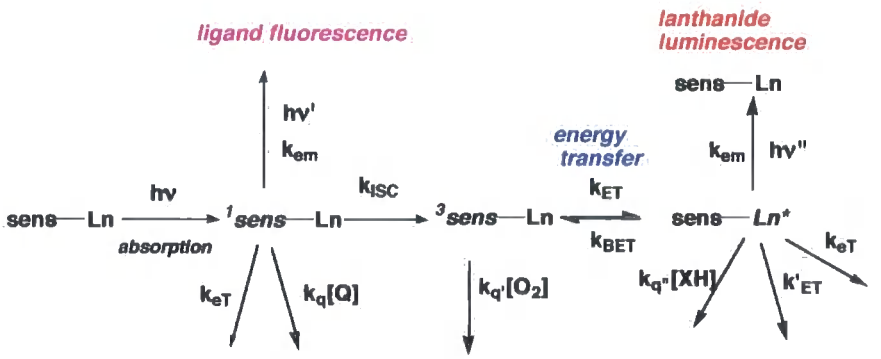

Figure 1.18 Photophysical processes

i) Quenching of the sensitiser singlet state – this could decay by fluorescence, preventing the desired intersystem crossing to form the sensitiser triplet state. The singlet state can also be perturbed by electron or charge transfer, resulting from intramolecular or intermolecular reactivity. Reversible binding processes such as protonation or metal binding to the chromophore can result in a change in the singlet excited state energy.

ii) Quenching of the sensitiser triplet state – the triplet state is particularly sensitive to quenching by molecular oxygen, resulting in the relaxation of the sensitiser to the ground state and formation of singlet oxygen.

iii) Quenching of the lanthanide emissive state – by vibrational energy transfer to oscillators of appropriate energy (for example O-H oscillators in water), or via electronic energy transfer.[28]

Deactivation of the lanthanide emissive state through vibrational energy transfer to proximate solvent molecules or the bound ligand, decreases the lifetime and intensity of lanthanide emission.[53] For europium (III) complexes, coupling occurs to the third vibrational overtone of the proximate OH oscillator whereas terbium (III) complexes couple with the fourth vibrational overtone (Figure 1.19). Windsor and Kropp demonstrated that effective luminescent quenching is inversely proportional to the energy gap between the lanthanide emissive and ground state; thus, quenching is less efficient for Tb^{3+} complexes, as a consequence of the Franck-Condon principle.[54]

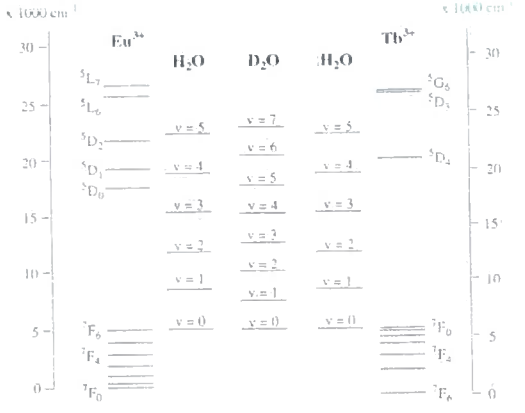

Figure 1.19 Energy level diagram for Eu^{3+} and Tb^{3+} with respect H_2O and D_2O oscillators

The deactivating energy transfer from the lanthanide emissive state into the vibrational energy of bonds is thought to occur via the Förster mechanism. The quenching of the lanthanide emissive state is subject to the proximity of the oscillator due to the r^{-6} distance dependence of the Förster mechanism. The most effective quenching oscillators are the amine NH ($\nu_{NH} \sim 3300cm^{-1}$) and OH bonds ($\nu_{OH} \sim 3400cm^{-1}$) as the O or N can coordinate directly to the lanthanide ion promoting the deactivating energy transfer. Amide NH ($\nu_{NH} \sim 3300cm^{-1}$) and CH ($\nu_{CH} \sim 2950cm^{-1}$) bonds have the smallest

contribution to quenching as they are further away from the lanthanide centre, so effective quenching is minimised due to r^{-6} dependence. The quenching effects of vibrational oscillators such as OH bonds have been investigated by the measurement of rate constants for the depopulation of the lanthanide emissive state in both H_2O and D_2O. As the corresponding deuteriated bonds have lower stretching frequencies, energy transfer occurs to higher vibrational states; so it is assumed that exchangeable XD oscillators do not contribute to the non-radiative deactivation of the lanthanides emissive state. Consequently, a comparison can be made between the rate constants, the difference being proportional to the quenching effect of the exchangeable XH oscillators. Therefore the number of water molecules coordinated to the metal centre can be calculated via the following equations, wherein the numerical correction term reflects the contribution of closely diffusing OH oscillators, for a typical hydrophilic complex.[55]

$$q_{Eu} = 1.2\ [(k_{H2O} - k_{D2O}) - 0.25]$$

$$q_{Tb} = 5\ [(k_{H2O} - k_{D2O}) - 0.06]$$

(Where 1.2 and 5 have the units of milliseconds)

Electron/charge transfers can also contribute to the non-radiative quenching of luminescence limiting the overall emission quantum yield. Electron transfer can occur from electron rich species present within cells, such as urate and ascorbate, quenching the long-lived lanthanide emissive state.

The Weller equation[56] can be utilised to estimate the thermodynamic feasibility of the quenching process:

$$\Delta G_{ET} = nF\ [(E_{ox} - E_{red}) - E^{Ln^*} - e^2/\ \varepsilon r]\ \text{J mol}^{-1}$$

where E_{ox} is the oxidation potential (versus NHE) of the electron donating quenching species, E_{red} is the reduction potential of the acceptor, either the chromophore or the metal, E^{Ln^*} is the energy of the lanthanide excited state and $e^2/\ \varepsilon r$ is a Coulombic attraction correction term associated with the formation of the transient ion pair.

Collisional quenching is described by the Stern–Volmer equation,

$$I_0/I = 1 + k_q \tau_0\ [Q] = 1 + K_{SV}\ [Q]$$

where I_0 and I are the fluorescence intensities (analogous to the lifetime) in the absence and presence of quencher, k_q is the bimolecular quenching constant, τ_0 is the lifetime of the fluorophore in the absence of the quencher and [Q] is the quencher concentration. Quenching species reduce the emission intensity and lifetime of the complex. The relative quenching ability may be defined by the related Stern-Volmer quenching constant, K_{sv}^{-1}. Assuming Stern Volmer quenching kinetics, the change in lifetime is measured as a function of concentration with the gradient of the plot giving the Stern Volmer quenching constant K_{sv}^{-1}. This represents the concentration of quencher required to reduce the lifetime or emission intensity down to 50% of its original value.[5]

Recent work within the Parker group has approached the study of the photoinduced electronic quenching of the lanthanide excited state. Figure 1.20 illustrates two typical cationic lanthanide complexes incorporating either an azaxanthone or tetraazatriphenylene chromophore. Table 1.2 contains Stern-Volmer quenching constants obtained for these complexes on addition of the quenching species; iodide, ascorbate and urate.[52 57]

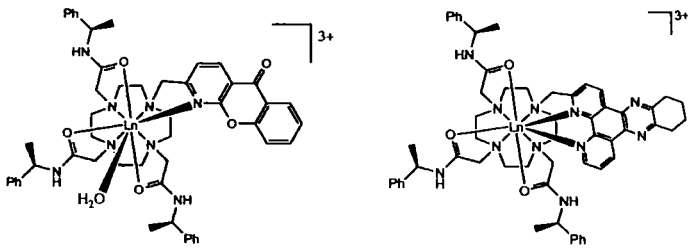

Figure 1.20 $[LnPh_3AzaH]^{3+}$ and $[LnPh_3dpqC]^{3+}$ respectively

Complex	K_{sv}^{-1} (mM) Iodide	K_{sv}^{-1} (mM) Ascorbate	K_{sv}^{-1} (mM) Urate
$[EuPh_3AzaH]^{3+}$	278	1.5	0.6
$[TbPh_3AzaH]^{3+}$	9.2	0.37	0.04
$[EuPh_3dpqC]^{3+}$	27	0.39	0.07
$[TbPh_3dpqC]^{3+}$	0.9	0.25	0.02

Table 1.2 Stern-Volmer quenching constants, K_{sv}^{-1} for $[LnPh_3AzaH]^{3+}$ and $[LnPh_3dpqC]^{3+}$ on addition of iodide, ascorbate or urate. (0.1M HEPES, 10μM Complex, 10mM NaCl, pH 7.4, 298K)

Quenching studies on tetraazatriphenylene and azaxanthone sensitised complexes have exhibited the following trends;[52]

i) The quenching for terbium complexes is far greater than that of europium, thought to be due to the higher free energy of Tb^{3+} ($^5D_4$ = 2.44 V) compared to that of Eu^{3+} ($^5D_0$ = 2.06 V), thus driving the electron transfer.

ii) Overall complex charge also has an impact on quenching with cationic complexes being most susceptible to quenching, followed by neutral and then anionic, consistent with the ordering of Coulombic repulsion in formation of the encounter complex (though this is most evident with iodide quenching). Steric bulk also has an inverse effect on quenching.

iii) Although ordering of quenching was expected to follow the ease of oxidation of the quenching anion,

Ascorbate (0.30 V) > Iodide (0.54 V) > Urate (0.59 V)[58]

experimentally, it was found that urate quenching is considerably more effective than anticipated.

iv) The azaxanthone (-1.1 V) sensitised complexes were less susceptible to the electron transfer than the tetraazatriphenylene (-1.6 V) analogues consistent with the ease of reduction.

Point iii) illustrates that there are other factors involved in the photoinduced electron transfer that could potentially be ascribed to either the structural or mechanistic influences of the quencher and their interaction with a given complex.

This work was also extended into the development of a ratiometric assay utilising the change in emission intensity in the presence of low molecular weight reductants. Two lanthanide complexes (Eu^{3+}/Tb^{3+}) incorporating a common ligand were mixed and the relative ratio of emission intensities of specific dominant bands provided a measure of

urate concentration. The measurements were both accurate and precise, when compared to the commonly used uricase enzyme kit assay.[59]

1.2.7 Hypothesis For The Proposed Work

This ratiometric assay demonstrates how the quenching of a luminescent complex can be utilised as a probe of the concentration of a given species. Therefore, with these quenching studies in mind, new luminescent lanthanide complexes were considered appropriate to be developed. These complexes should incorporate a quenching moiety in order to reduce luminescence; this 'quenched' complex will then be applied as a ratiometric probe by permutation of the Ln^{3+} ion. When the complex comes into contact with reactive oxygen species, it should act as an 'off/on' switch, as the extent of quenching by the electron donor should be reduced by preferential electron transfer with the ROS, thereby increasing complex luminescence (Figure 1.21).

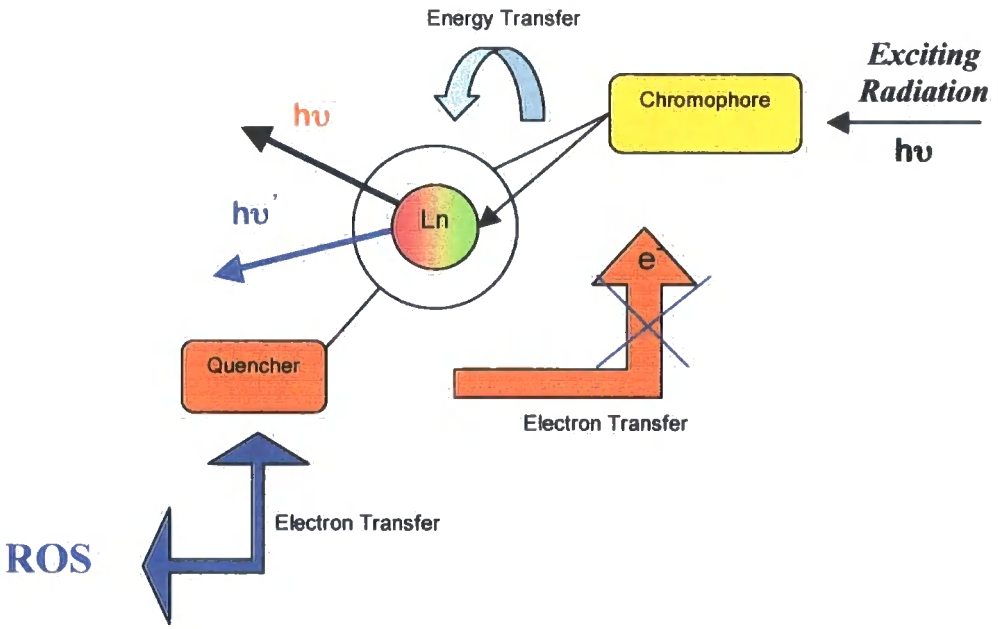

Figure 1.21 Schematic representation of a 'quenched' complex and the potential electron transfer occurring in the presence of ROS, resulting in increased luminescence

In this work, it is proposed to develop complexes incorporating a quenching moiety based on a derivative of ascorbate, urate or a catecholate. It is important that this quenching moiety is able to react rapidly with ROS, thus relaying the effect to the luminescence of the complex, which will provide a measure of relative ROS

concentration. This should also be a reversible process. When a more powerful reductant such as ascorbate is present or is added, the luminescence should again decrease back to the 'quenched' value. Complexes of Eu^{3+} and Tb^{3+} should, on the basis of previous quenching studies, respond to both the incorporated quencher and the presence of ROS to different degrees, thus enabling a ratiometric measurement. Such a hypothetical system requires that the rate of oxidation of the 'electron-rich' quenching moiety in the probe is fast with respect to the direct scavenging of the ROS by ascorbate.

References

[1] B. Halliwell and J. M. C. Gutteridge, in *Free Radicals in Biology and Medicine*, Oxford University Press, 2007, 4th Ed

[2] S. P. Colowick and N. O. Kaplan, in *Methods in Enzymology*, Academic Press, Inc., 1984, Vol. 105: Oxygen Radicals in Biological Systems

[3] G. Bartosz, *Clin. Chim. Acta*, **368**, 2006, 53

[4] N. Soh, *Anal. Bioanal. Chem.*, **386**, 2006, 532

[5] J. R. Lakowicz, in *Principles of Fluorescence Spectroscopy*, Kluwer Academic/Plenum Publishers, 1999, 2nd Ed., p. 53

[6] S. Kenston and R. Brandt, *Anal. Biochem.*, 1965, **11**, 1

[7] a) C. P. LeBel, H. Ischiropoulos and S. C. Bondy, *Chem. Res. Toxicol.*, 1992, **5**, 227; b) S. L. Hempel, G. R. Buettner, Y. Q. O'Malley, D. A. Wessels and D. M. Flaherty, *Free Radical Biol. Med.*, 1999, **27**, 146

[8] L. A. MacManus-Spencer, D. E. Latch, K. M. Kroncke and K. McNeill, *Anal. Chem.*, 2005, **77**, 4, 1200

[9] K. Tanaka, T. Miura, N. Umezawa, Y. Urano, K. Kikuchi, T. Higuchi and T. Nagano, *J. Am. Chem. Soc.*, 2001, **123**, 2530

[10] a) B. Song, G. Wang, J. Yuan, *Chem. Commun.*, 2005, 3553; b) B. Song, G. Wang, M. Tan and J. Yuan, *New J. Chem.*, 2005, **29**, 1431

[11] B. Song, G. Wang, M. Tan and J. Yuan, *J. Am. Chem. Soc.*, 2006, **128**, 13442

[12] M. Onoda, H. Tokuyama, S. Uchiyama, K. Mawatari, T. Santa, K. Kaneko, K. Imai and K. Nakagomi, *Chem. Commun.*, 2005, 1848

[13] a) O. S. Wolfbeis, A. Dürkop, M. Wu and Z. Lin, *Angew. Chem. Int. Ed.*, 2002, **41**, 23, 4495; b) V. N. Kozhevnikov, C. Mandl, S. Miltschitzky, A. Duerkop, O. S. Wolfbeis and B. Koenig, *Inorg. Chim. Acta.*, 2005, **358**, 2445

[14] H. Maeda, Y. Fukuyasu, S. Yoshida, M. Fukuda, K. Saeki, H. Matsuno, Y. Yamauchi, K. Yoshida, K. Hirata and K. Miyamoto, *Angew. Chem. Int. Ed.*, 2004, **43**, 2389

[15] M. C. Y. Chang, A. Pralle, E. Y. Isacoff and C. J. Chang, *J. Am. Chem. Soc.*, 2004, **126**, 15392

[16] E. W. Miller, A. E. Albers, A. Pralle, E. Y. Isacoff and C. J. Chang, *J. Am. Chem. Soc.*, 2005, **127**, 16652

[17] A. E. Albers, V. S. Okreglak and C. J. Chang, *J. Am. Chem. Soc.*, 2006, **128**, 9640

[18] H. Maeda, K. Yamamoto, Y. Nomura, I. Kohno, L. Hafsi, N. Ueda, S. Yoshida, M. Fukuda, Y. Fukuyasu, Y. Yamauchi and N. Itoh, *J. Am. Chem. Soc.*, 2005, **127**, 68

[19] B. Heyne, C. Beddie and J. C. Scaiano, *Org. Biomol. Chem.*, 2007, **5**, 1454

[20] K. Setsukinai, Y. Urano, K. Kikuchi, T. Higuchi and T. Nagano, *J. Chem. Soc., Perkin Trans. 2*, 2000, 2453

[21] K. Setsukinai, Y. Urano, K. Kakinuma, H. J. Majima and T. Nagano, *J. Biol. Chem.*, 2003, **278**, 5, 3170

[22] N. Soh, K. Makihara, E. Sakoda and T. Imato, *Chem. Commun.*, 2004, 496

[23] R. A. Poole, C. Montgomery, E. J. New, D. Parker and A. Congreve, *Org. Biomol. Chem.*, 2007, **5**, 2055

[24] A. D. Sherry and C. F. G. Geraldes, in *Lanthanide Probes in Life, Chemical and Earth Sciences*, J. G. Bunzli and G. R. Choppin, Elsevier, Amsterdam, 1989, p. 219

[25] D. F. Shriver and P. W. Atkins, in *Inorganic Chemistry*, Oxford University Press, 2001, 3rd ed., p. 321

[26] N. N. Greenwood and A. Earnshaw, in *Chemistry of the Elements*, Butterworth-Heinemann, 1998, 2nd ed., p. 1242

[27] J. I. Bruce, M. P. Lowe and D. Parker, in *The Chemistry of Contrast Agents in Medical Magnetic Resonance Imaging*, A. Merbach and E. Toth, John Wiley & Sons Ltd., 2001, p. 437

[28] D. Parker and J. A. G. Williams, in *Metal Ions in Biological Systems*, A. Sigel and H. Sigel, Marcel Dekker., New York and Basel, 2003, vol. 40, p. 233

[29] W. T. Carnall, in *Handbook on the Physics and Chemistry of Rare Earths*, K. A. Gschneider and L. Eyring, Elsevier, 1998, vol. 25, p. 171

[30] D. Parker, *Coord. Chem. Rev.*, 2000, **205**, 109

[31] a) M. F. Reid and F. S. Richardson, *J. Chem. Phys.*, 1983, **79**, 5735; b) A. F. Kirby, D. Foster and F. S. Richardson, *Chem. Phys. Lett.*, 1983, **95**, 507

[32] J. I. Bruce, D. Parker and D. J. Tozer, *Chem. Commun.*, 2001, 2250

[33] D. Parker, R. S. Dickins, H. Puschmann, C. Crossland and J. A. K. Howard, *Chem. Rev.*, 2002, **102**, 1977

[34] S. I. Weissman, *J. Chem. Phys.*, 1942, **10**, 214

[35] D. Parker and J. A. G. Williams, *J. Chem. Soc., Dalton Trans.*, 1996, 3613

[36] T. Förster, *Discuss. Faraday Soc.* 1959, **27**, 7

[37] D. L. Dexter, *J. Chem. Phys.*, 1953, **21**, 836

[38] S. I. Klink, *Synthesis and Photophysics of Light-Converting Lanthanide Complexes*, PhD Thesis, University of Twente, 2000

[39] S. Pandya, J. Yu and D. Parker, *Dalton Trans.*, 2006, 2757

[40] M. H. V. Werts, R. T. F. Jukes and J. W. Verhoeven, *Phys. Chem. Chem. Phys.*, 2002, **4**, 1542

[41] J. W. Steed and J. L. Atwood, in *Supramolecular Chemistry*, John Wiley & Sons Ltd., 2000, p. 9

[42] S. Lis, M. Elbanowski, B. Mąkowska and Z. Hnatejko, *J. Photochem. Photobiol. A: Chem.*, 2002, **150**, 233

[43] R. S. Dickins, D. Parker, J. I. Bruce and D. J. Tozer, *Dalton Trans.*, 2003, 1264

[44] D. Parker, *Chem. Soc. Rev.*, 2004, **33**, 156

[45] a) E. B. van der Tol, H. J. Ramesdonk, J. W. Verhoeven, F. J. Skeemers, E. G. Kever, W. Verboom and D. N. Reinhoudt, *Chem. Eur. J.*, 1998, **4**, 1935; b) B. H. Bakker, M. Goes, N. Hoebe, H. J. van Ramesdonk, J. W. Verhoeven, M. H. V. Werts, J. W. Hofstraat, *Coord. Chem. Rev.*, 2000, **208**, 3; c) S. Quici, G. Marzanni, M. Cavazzini, P. L. Anelli, M. Botta, E. Gianolio, G. Accorsi, N. Armaroli and F. Barigelletti, *Inorg. Chem.*, 2002, **41**, 2777

[46] a) G. Bobba, J-C. Frias and D. Parker, *Chem. Commun.*, 2002, 890; b) G. Bobba, *Interaction of Chiral Lanthanide Complexes with Nucleic Acids*, PhD Thesis, University of Durham, 2002; c) J-C. Frias, G. Bobba, M. J. Cann, C. J. Hutchison and D. Parker, *Org. Biomol. Chem.*, 2003, **1**, 905; d) G. Bobba, Y. Bretonnière, J-C. Frias and D. Parker, *Org. Biomol. Chem.*, 2003, **1**, 1870; e) R. A. Poole, G. Bobba, M. J. Cann, J-C. Frias, D. Parker and R. D. Peacock, *Org. Biomol. Chem.*, 2005, **3**, 1013

[47] A. Dadabhoy, S. Faulkner and P. G. Sammes, *J. Chem. Soc., Perkin Trans. 2*, 2000, 2359

[47] A. Dadabhoy, S. Faulkner and P. G. Sammes, *J. Chem. Soc., Perkin Trans. 2*, 2002, 348

[48] A. Beeby, L. M. Bushby, D. Maffeo and J. A. G. Williams, *J. Chem. Soc., Perkin Trans. 2*, 2000, 1281

[49] A. Beeby, L. M. Bushby, D. Maffeo and J. A. G. Williams, *J. Chem. Soc., Dalton Trans.*, 2002, 48

[50] P. Atkinson, K. S. Findlay, F. Kielar, R. Pal, R. A. Poole, H. Puschmann, D. Parker, S. L. Richardson, P. A. Stenson, A. L. Thompson and J. Yu, *Org. Biomol. Chem.*, 2006, **4**, 1707

[51] a) D. Parker and J. Yu, *Chem. Commun.*, 2005, 3141; b) D. Parker and J. Yu, *Eur. J. Org. Chem.*, 2005, 4249; c) J. Yu, D. Parker, R. Pal, R. Poole and M. Cann, *J. Am. Chem. Soc.*, 2006, **128**, 2294

[52] R. A. Poole, *Luminescent Lanthanide Complexes for Cellular Applications*, PhD Thesis, University of Durham, 2006

[53] R. S. Dickins, D. Parker, A. S. de Sousa and J. A. G. Williams, *Chem. Commun.*, 1996, 697

[54] a) J. L. Kropp and M. W. Windsor, *J. Chem. Phys.*, 1963, **39**, 2769; b) J. L. Kropp and M. W. Windsor, *J. Chem. Phys.*, 1965, **42**, 1599

[55] A. Beeby, I. M. Clarkson, R. S. Dickins, S. Faulkner, D. Parker, L. Royle, A. S. de Sousa, J. A. G. Williams and M. Woods, *J. Chem. Soc., Perkin Trans. 2*, 1999, 493

[56] A. Weller, *Pure Appl. Chem.*, 1968, **16**, 115

[57] 4th year MChem report, S. L. Richardson, University of Durham, 2006

[58] a) S. Steenken and P. Neta, *J. Phys. Chem.*, 1982, **86**, 3661; b) G. R. Buettner, *Arch. Biochem.Biophy.*, 1993, **300**, 535

[59] R. A. Poole, F. Kielar, S. L. Richardson, P. A. Stenson, D. Parker, *Chem. Commun.*, 2006, 4084

Figures – Authors own, except figures; 1.12, 1.13, 1.14, 1.18, and 1.19 courtesy of D. Parker.

2. Synthesis

The proposed complexes will comprise a 1,4,7,10-tetraazacyclododecane macrocycle, incorporating two coordinating arms, a quenching moiety, and a common chromophore group. The quenching moiety and chromophore will be held in close proximity to one another via the backbone structure and coordination to the lanthanide centre (Figure 2.1).

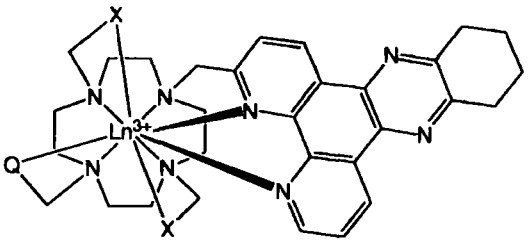

Figure 2.1 Target molecular structure, where Ln^{3+}=Eu or Tb; X = Coordinating arms, either carboxylate or amide; Q = Urate or Catecholate Moiety

The 1,4,7,10-tetraazacyclododecane macrocycle was selected as the backbone of the ligand, possessing four ring nitrogens that could be readily alkylated. Carboxylate groups were chosen as the two coordinating arms, with a tetraazatriphenylene sensitiser at the third position and a quenching moiety at the fourth. The quenching moiety was chosen based on its ability to quench the lanthanide-excited state; on the basis of both oxidation potential and quenching measurements (see Section 3.1.4; pg. 44). Studies implied uric acid and catechol derivatives were initially considered to be promising quenching moieties for ligand incorporation.

2.1 Synthesis of Uric Acid Derivatives[1]

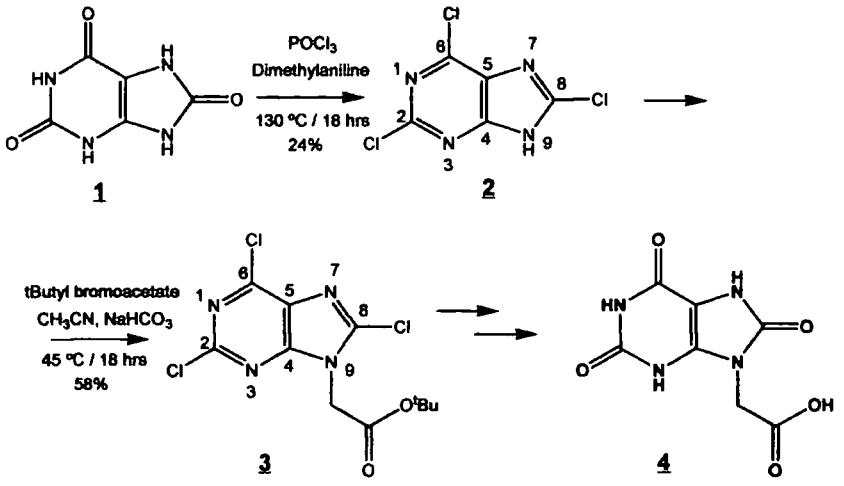

Scheme 2.1 Synthesis of uric acid derivatives and the target system in bold

The attachment of urate to the ligand required selective N-functionalisation of the ring system (Scheme 2.1). Uric acid, **1**, was first converted to the chlorinated derivative, **2**, via reaction with phosphoryl chloride and dimethylaniline, which would allow N-alkylation of the imidazole ring (N^7 or N^9). The chlorinated product was highly insoluble in all solvents thus preventing solution-state NMR analysis, and proved not to be amenable to characterisation by ESMS. The nature of the product was only confirmed by the melting point and elemental analysis; a marked change in melting point was observed from > 250 °C for uric acid, to 176 – 178 °C for 2,6,8-trichloropurine. The presence of the three chlorines was confirmed by elemental analysis.

The methylation of trichloropurine, originally pioneered by Fischer[2], is well known. For the alkylation of 2,6,8-trichloropurine relatively gentle conditions were used, due to the high reactivity of *tert*-butylbromoacetate. Initially, the reaction was performed in DMF in the presence of K_2CO_3 but this resulted in an ill-defined reaction. The reaction was then performed in MeCN using $NaHCO_3$ as a milder base. The alkylation reaction under these conditions resulted in the formation of the 2 constitutional isomers, **3**, that were separated using column chromatography with a hexane:ethyl acetate gradient system. The alkylation reaction did not go to completion, and other species appeared to be formed when the reaction was left for extended periods. Each of these reactions was also low yielding which may be a consequence of the insolubility of uric acid

derivatives. Following removal of the *tert*-butyl group with TFA (20 °C, 18 hrs), it appeared as though the ring system was opening. Monitoring by TLC showed 1 spot → 4 spot for the N9 analogue and 1 spot → 3 spots for the N7 analogue, with the number of CH_2 peaks on the NMR following the same pattern. Thus, it seemed that TFA may have been too strong an acid to use on the system. Treatment with concentrated hydrochloric acid (100 °C, 18 hrs) yielded no change. Therefore, the trichloropurine was heated in the presence of strong base (100 °C, 18 hrs). Once again, a series of products was obtained which could not be easily assigned, and it was thought that perhaps either the ring had been destroyed or partial dechlorination of the compound was occurring, as some of the isotope patterns were consistent with the presence of two chlorines instead of three. Many of the problems arising from these reactions can perhaps be explained by the relative insolubility of these compounds. Due to the systematic difficulties associated with the manipulation of uric acid derivatives, the catechols were seen as a more promising alternative.

2.2 Synthesis of Catechol Derivatives[3]

Catechol derivatives are more accessible than those of uric acid, and as the quenching ability was considered to be reasonable for the protected catechol, as well as the free catechol, their substitution and integration into ligand systems was attempted.

Catechols need to be protected for many chemical transformations, owing to the facility of oxidation in solution. Such solution instability in aerated aqueous media was also noted during the quenching studies (see Section 3.1.4; pg. 44). Methylene protection is difficult to remove, whereas an acetonide derivative may be more easily hydrolysed under acidic conditions. Initially, the dimethylmethylene analogue of 3,4-dihydroxyhydrocinnamic acid was synthesised (Scheme 2.2).

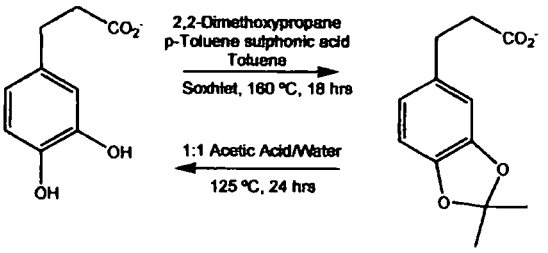

Scheme 2.2 Protection and deprotection of 3,4-hydroxycinnamic acid

The reaction of the free catechol with 2,2-dimethoxypropane under Soxhlet conditions yielded the protected catechol. Although this stable analogue could be easily deprotected in the presence of acetic acid, initially it was considered desirable to have an amine chain as a linker group rather than an acid, so that a relatively shorter linker could be used for cyclen attachment.

Amines such as dopamine cannot be protected under conditions such as those above due to the amine nucleophilicity; therefore the cyclen linker chain was first attached (Scheme 2.3).

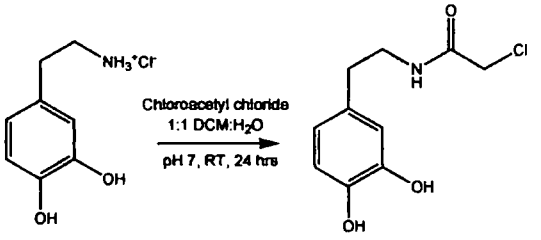

Scheme 2.3 Selective N-acylation of Dopamine

Though this selective N-acylation reaction was successful, the product was only soluble in solvents such as methanol, water and acetone. Therefore, selective protection of the phenolic groups with an acetonide group was not straightforward. For example, hydrolysis would result in a reversible reaction back to the starting materials.

On further consideration of the oxidation of free catechols, it was thought that perhaps integrating a quenching moiety that could be easily deprotected to its oxidisable form under aqueous conditions (an irreversible reaction), might be detrimental to the 'quenched complex'. Therefore, since the methylene-protected catechols had shown some tendency to quench the lanthanide excited state (see Section 3.1.4; pg. 44) and were stable with respect to oxidation under aqueous conditions, these were chosen for incorporation into the ligand (Scheme 2.4).

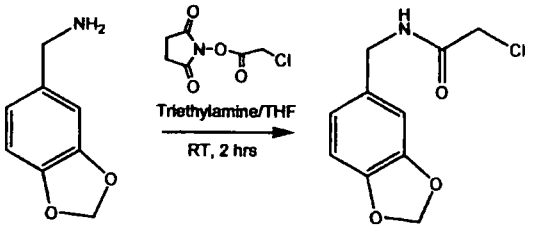

Scheme 2.4 Acylation of 3,4-methylenedioxybenzylamine

Reaction of 3,4-methylenedioxybenzylamine with 1-(2-chloroacetyl)pyrrolidine-2,5-dione yielded a linkable arm for addition to the cyclen ligand.

2.3 Ligand and Complex Synthesis[4]

The synthesis of the prototype ligand that incorporates a macrocyclic ligand for Ln (III) ion binding and an internal quenching moiety is given in Scheme 2.5.

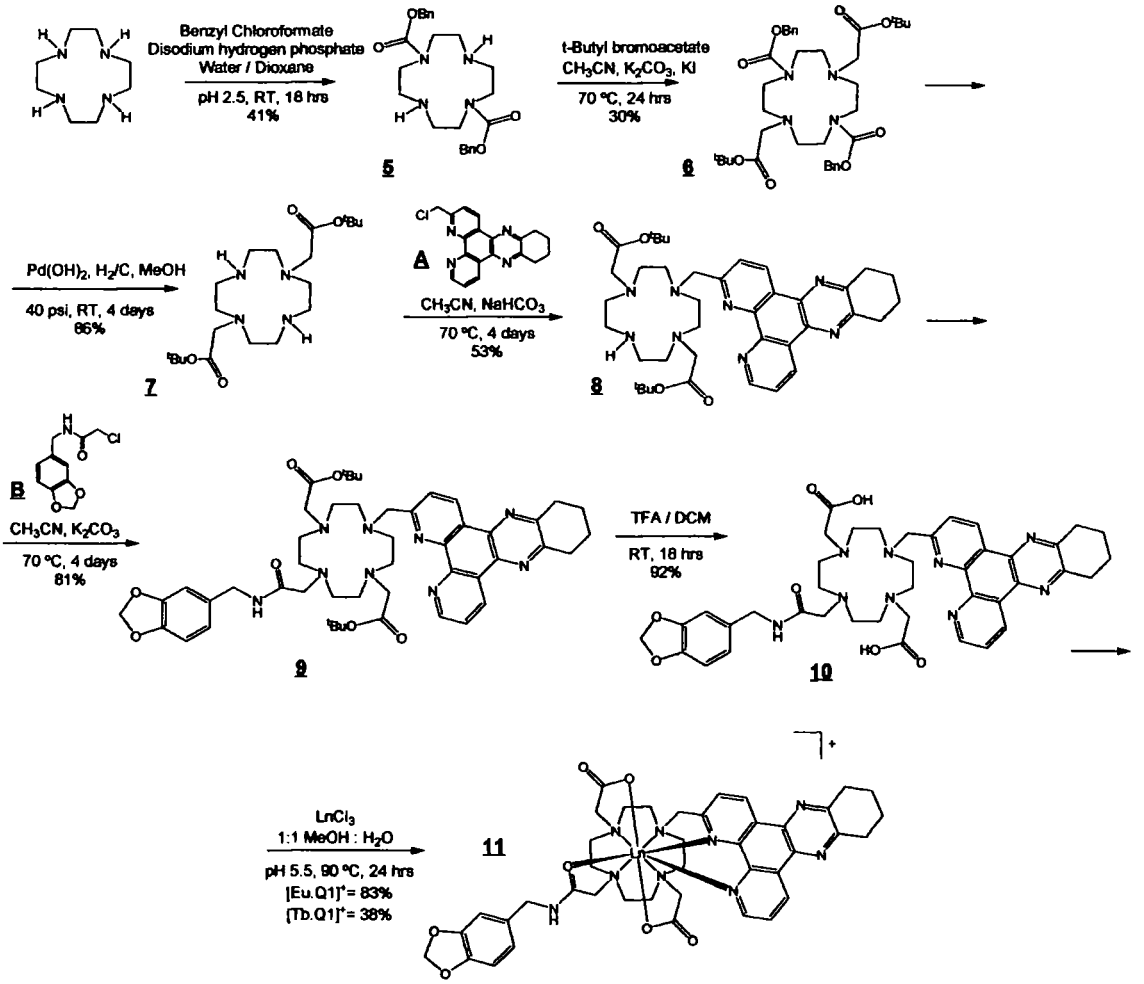

Scheme 2.5 Ligand and complex synthesis of $[Eu.Q1]^+$ and $[Tb.Q1]^+$

The bis-carbonate, **5**, was heated in the presence of 2.4 equivalents of *tert*-butylbromoacetate in the presence of base and a catalytic amount of KI. The product obtained was the desired tetrasubstituted cyclen, **6**. Unfortunately, a large amount of quaternary salt was also formed resulting in a relatively low yield. The 'cbz' groups were removed by hydrogenation in the presence of palladium hydroxide over carbon to yield the amine, **7**.

The monoalkylation of the ligand with **A** was firstly performed in acetonitrile in the presence of potassium carbonate but this resulted in disubstitution. Various conditions were used in an attempt to minimise the degree of disubstitution; different solvents (chloroform and ethanol) and different temperatures were experimented with. Eventually, it was found that the highest conversion to the desired monosubstituted product, **8**, could be achieved using a weaker base, such as $NaHCO_3$. This was found to be a rather slow reaction taking days to reach completion. Use of any more than 1.5 equivalents of base led to the formation of the disubstituted ring system. The crude product was purified by column chromatography to remove any excess **A**. The quenching amide arm, **B**, was reacted with **8** in acetonitrile in the presence of Cs_2CO_3; this reaction was also slow to reach completion. Purification at this stage was undertaken via a series of aqueous washings, as column chromatography was shown to retain a lot of the ligand. Deprotection of **9** was performed with TFA, and subsequent complexation of **10** with $LnCl_3$ in water at pH 5.5 yielded the desired complexes, **11** (Ln=Eu or Tb), as confirmed by mass spectrometry, HPLC and photophysical measurements (Figure 2.2; also see Section 3.2; pg. 49 and Section 5.2; pg. 78)

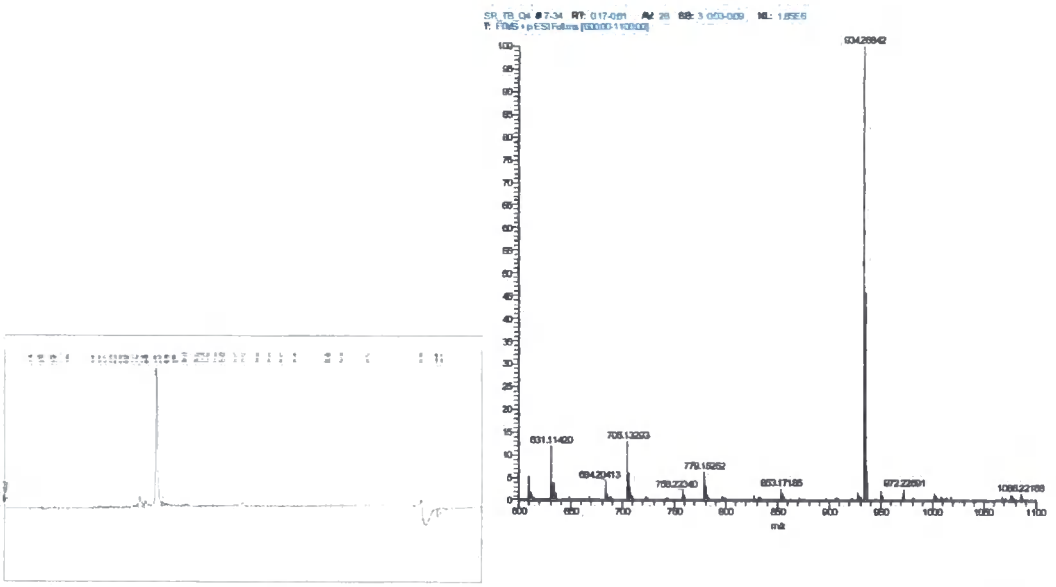

Figure 2.2 HPLC chromatogram (absorbance at 254 nm vs. time) and mass spectrum of [Tb.Q1]

References

[1] J. Davoll and B. A. Lowy, *J. Am. Chem. Soc.*, 1951, **73**, 2936

[2] E. Fischer, *Ber.*, 1897, **30**, 2220

[3] T. W. Greene and P. G. M. Wuts, in *Protective Groups in Organic Synthesis*, John Wiley & Sons Ltd., 1999, 3rd Ed., p.287

[4] Z. Kovacs and A. D. Sherry, *J. Chem Soc., Chem. Commun.*, 1995, 185

3. Results and Discussion

3.1 Quenching of the Lanthanide Excited State

Quenching studies previously undertaken by the Parker group have demonstrated some intriguing trends (see Section 1.2.6; pg. 24). Further work described herein seeks to develop a model to define the charge or electron transfer process between lanthanide complexes and the quenching species, resulting in a reduction in both the lifetime and emission intensity of the complex.

Ascorbate and urate are important anti-oxidants abundant within the human body (Scheme 3.1).[1] Previous work has examined the quenching of luminescence of various europium and terbium complexes in the presence of these low molecular weight anti-oxidants.[2]

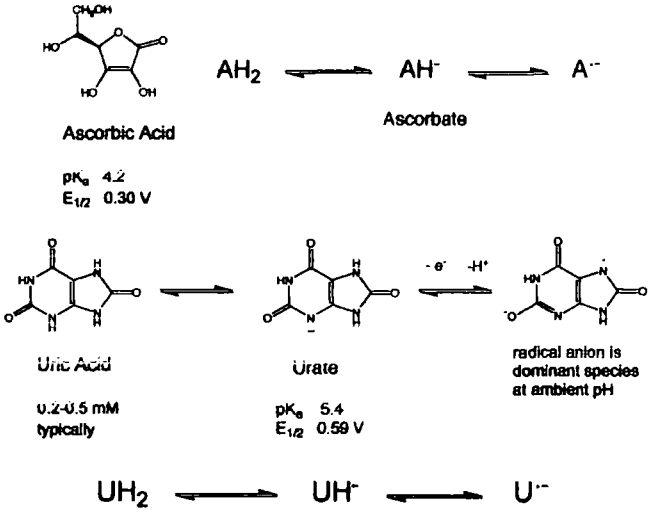

Scheme 3.1 Ascorbate and Urate Characteristics

Couple	E^0 (V) pH 7
$HU^{\bullet-}$, H^+ / UH_2 (Urate)	0.59
Catechol-$O^{\bullet}$, H^+ / Catechol-OH	0.53
Ascorbate$^{\bullet}$, H^+ / ascorbate monoanion	0.30

Table 3.1 One-electron oxidation potentials for a series of low molecular weight oxidants (298K, pH 7.4).[1]

One electron potentials are important in considering possible quenching species, as the oxidation potential of the quencher relates how easily an electron is transferred to a chromophore (Table 3.1). As observed from previous studies, urate quenching was more effective than anticipated from its one electron oxidation potential. This behaviour may relate to its ability to π-π stack with the chromophore, thereby promoting the formation of a longer lived encounter complex or exciplex. Though the extent of quenching does not necessarily follow the oxidation pecking order, as observed via the extent of urate quenching, the electron potentials still provide a speculative measure.

Each of the quenching studies was performed on the complex $[TbPh_3AzaH]^{3+}$ (unless otherwise stated), which had previously been synthesised (Figure 3.1) by the author.

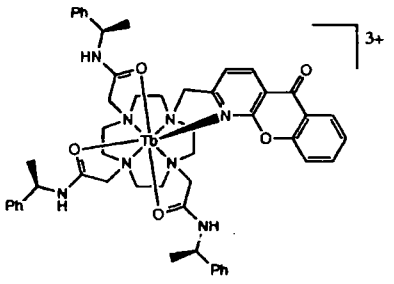

Figure 3.1 $[TbPh_3AzaH]Cl_3$

3.1.1 Stern-Volmer Quenching Constants

Collisional quenching occurs when a fluorophore and quencher interact. This can lead to collisional (dynamic quenching) and/or static quenching. For collisional quenching, the complex and quencher must interact within the lifetime of the excited state. Upon contact the fluorophore will return to the ground state without emission of a photon. For static quenching, the fluorophore and quencher form a complex which is non-fluorescent.

Collisional quenching is described by the Stern–Volmer equation, eq (1):

$$I_0/I = 1 + k_q \tau_0 [Q] = 1 + K_D [Q] \qquad (1)$$

where I_0 and I are the fluorescent intensities in the absence and presence of quencher; k_q is the bimolecular quenching constant; τ_0 is the lifetime of the fluorophore in the

absence of the quencher and [Q] is the quencher concentration. The Stern–Volmer quenching constant is given by $k_q \tau_0$ named either K_D or K_{SV} depending on whether the quenching is known to be dynamic. A Stern–Volmer plot is therefore a plot of I_0/I against [Q] where K_{SV} is the slope of the graph. The reciprocal constant, K_{SV}^{-1} is the concentration at which 50% of the intensity is quenched. The bimolecular quenching constant, $k_q = f_Q\ k_o$, where f_Q is the quenching efficiency and k_o is the diffusion controlled bimolecular rate constant, where the quenching efficiency and its limitation vary with complex structure.[3]

For collisional quenching, the relative decrease in lifetime is equivalent to that of the fluorescence intensity as it also represents the excited state being depopulated without emission. It should be noted that static quenching does not decrease the lifetime of a complex as only fluorescent molecules are observed in lifetime measurements.

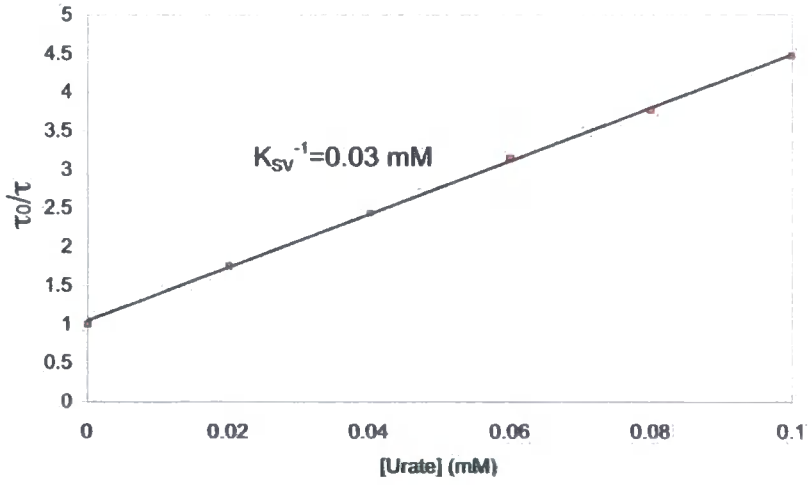

Figure 3.2 Typical example of a Stern-Volmer plot used to obtain a value for the Stern-Volmer quenching constant K_{sv}^{-1}. (0.1M HEPES, 10μM $TbPh_3AzaH^{3+}$, 10mM NaCl, pH 7.4, 298K).[4]

A linear Stern–Volmer plot, e.g. (Figure 3.2) is generally indicative of a single class of fluorophore where all are equally accessible to quencher. Therefore deviations from linearity show more than one fluorophore population where one or more classes are not as accessible to quencher, thus deviating towards the x-axis. During previous studies there were Stern-Volmer plots which showed a curvature away from linear Stern-Volmer kinetics, where above a certain value of quencher concentration a limiting value of τ_0/τ was reached.

3.1.2 Extended Range Stern-Volmer Plots

Lifetime measurements with ascorbate, urate and a series of catechols were extended by increasing the concentration range to examine the behaviour for higher concentration ranges of the quencher. The magnitude of the τ_0/τ limit was hoped to reveal information on quenching, as the extent of quenching (K_{SV}^{-1}) was not necessarily dependent on the limiting value of τ_0/τ.

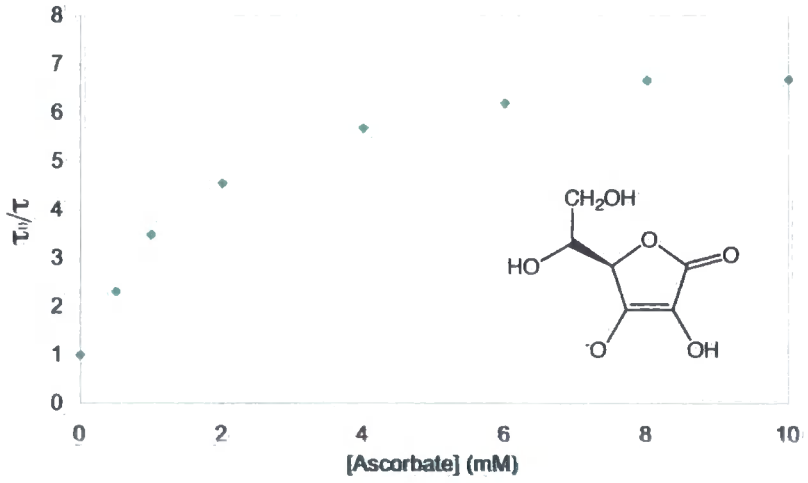

Figure 3.3 Stern–Volmer plot for the quenching of $[TbPh_3AzaH]^{3+}$ by ascorbate (0.1M HEPES, 10μM $TbPh_3AzaH^{3+}$, 10mM NaCl, pH 7.4, 298K)

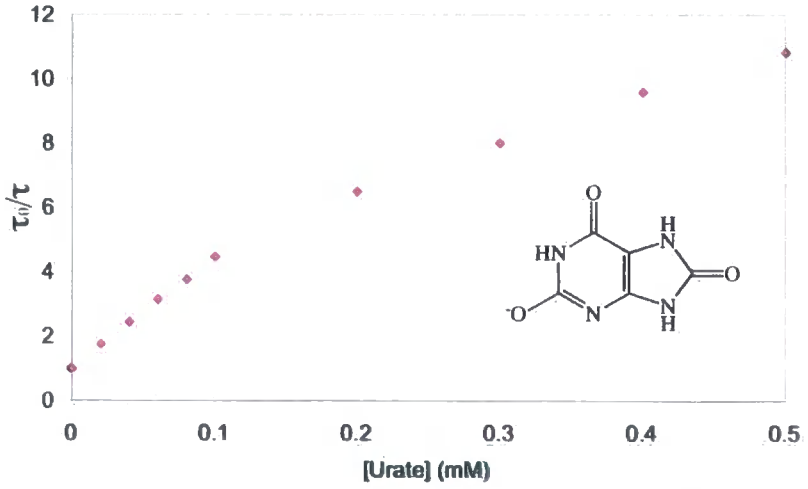

Figure 3.4 Stern–Volmer plot for the quenching of $[TbPh_3AzaH]^{3+}$ by urate (0.1M HEPES, 10μM $TbPh_3AzaH^{3+}$, 10mM NaCl, pH 7.4, 298K)

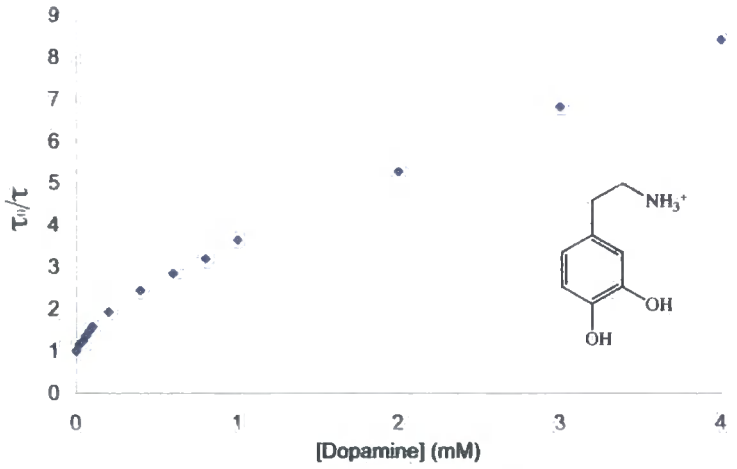

Figure 3.5 Stern–Volmer plot for the quenching of $[TbPh_3AzaH]^{3+}$ by dopamine (0.1M HEPES, 10μM $TbPh_3AzaH^{3+}$, 10mM NaCl, pH 7.4, 298K)

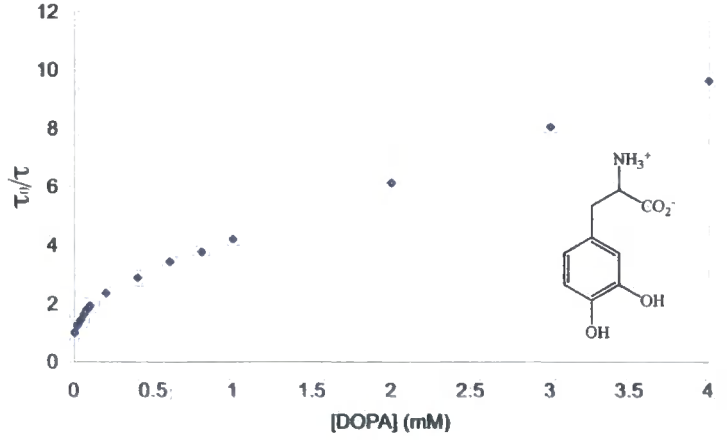

Figure 3.6 Stern–Volmer plot for the quenching of $[TbPh_3AzaH]^{3+}$ by DOPA (0.1M HEPES, 10μM $TbPh_3AzaH^{3+}$, 10mM NaCl, pH 7.4, 298K)

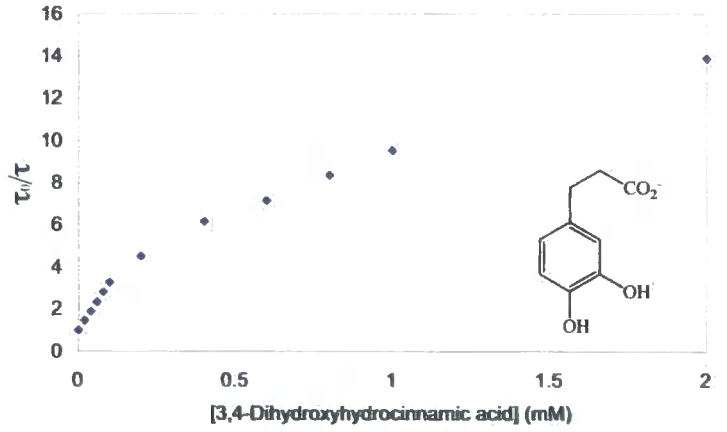

Figure 3.7 Stern–Volmer plot for the quenching of $[TbPh_3AzaH]^{3+}$ by 3,4-dihydroxyhydrocinnamate (0.1M HEPES, 10μM $TbPh_3AzaH^{3+}$, 10mM NaCl, pH 7.4, 298K)

As can be seen from the above plots, in every case the gradient changes with increasing concentration. Unfortunately, the experimental limit was reached before a limiting τ_0/τ value could be measured. Ascorbate appears to be close to its limiting value, reaching a plateau at ~ 8mM (τ_0/τ =6.7), with the other graphs progressing towards their limits. An interesting observation is that the catechol Stern-Volmer plots show the same odd gradient change, almost a second linearity suggesting a secondary mechanism at higher concentrations. Although deviation from Stern-Volmer kinetics is apparent for $[TbPh_3AzaH]^{3+}$ in the presence of each of these 'quenchers' this is not the case for every complex (see Section 3.1.4; pg. 45); as shown in preliminary studies, neutral and anionic complexes appear to not show this non-linearity as consistently as the cationic series of complexes.

At higher quencher concentrations for ascorbate and urate, the experimental exponential curves characterising the decay of the terbium excited state showed deviation from simple to multi-exponential decay to various degrees for different species. The curves initially still exhibited a well-defined shorter-lived component (following the curvature of the Stern-Volmer plot) but then showed a longer-lived component closer to that of the free complex. For the SV plots, the shorter-lived component was used to estimate the lifetime.

3.1.3 Ionic Strength Dependence

When reactions occur in a solution of finite ionic strength, generally only those between the reactant pairs are considered; at high concentrations this approximation becomes inaccurate. Non-reactive ions can often influence the reaction especially when the reactants are charged, as this serves to define the activity and chemical potential of the ion. Therefore, the sensitivity of urate and iodide quenching was studied at various ionic strengths, using NaCl to modulate the total ionic strength of the solution.

At low ionic strength, the activity coefficient of an ion may be estimated from the limiting Debye-Hückel equation;

$$\mathrm{Log}_{10}\gamma_A = -A' z_A^2 \sqrt{I}$$

In aqueous solution at 298K, A'=0.509 $dm^{3/2}mol^{-1/2}$, thus;

$$Log_{10}(k/k_0) = 1.018\ z_A z_B \sqrt{I}$$

k_0 is equal to $k_r K_{AB}$, and is the rate constant at zero ionic strength. This equation holds experimentally as long as the ionic strength is not too high ($<10^{-2}$ $moldm^{-3}$). A plot of logk versus $\sqrt{I}$ gives a straight-line plot with slope $\sim z_A z_B$, so the rate increases with [I] for reactants of like charge and decreases for oppositely charged ions. Debye-Hückel theory is based upon a model where the chemical potential of the central ion is lowered by partial neutralisation of its charge, this is due to each ion being surrounded by an ionic atmosphere of equal but opposite charge. Therefore if A and B have like charges then high ionic strength will favour formation of the highly charged encounter pair and will increase the reaction rate.[5]

The quenching behaviour was examined as a function of I, in an attempt to glean information about the encounter complex formed between the Tb (III) complex and a quenching moiety. The complex studied was triply charged so the influence of ions in solution will bear more of an impact than for a neutral complex. The terbium lifetime for $[TbPh_3AzaH]^{3+}$ was monitored as NaCl was added, in the range 0 mM to 800 mM. A control experiment was performed initially to examine the lifetime variation in the absence of the quencher. The quencher concentration was kept constant, with a value chosen to fall within the linear Stern-Volmer range (40 μM for urate, 10 mM for iodide).

The lifetime of the free complex decreased with increasing ionic strength (1.5 ms to 1.25 ms), whereas the lifetime of the complex in the presence of the 'quenchers' increased with increasing ionic strength (Figure 3.8). The chloride ions will be drawn towards the cationic complex via Coulombic attraction, surrounding the complex and inhibiting approach of the quencher. This process disfavours exciplex or encounter complex formation. The effect was much more pronounced for iodide. It exhibited a classical salt effect, in that the collisional encounter between ions of opposite charge was observed to be sensitive to local ionic strength. The ionic strength dependence appears to reach a limit at 400 mM NaCl, with increasing ionic strength having no further effect on the lifetime.

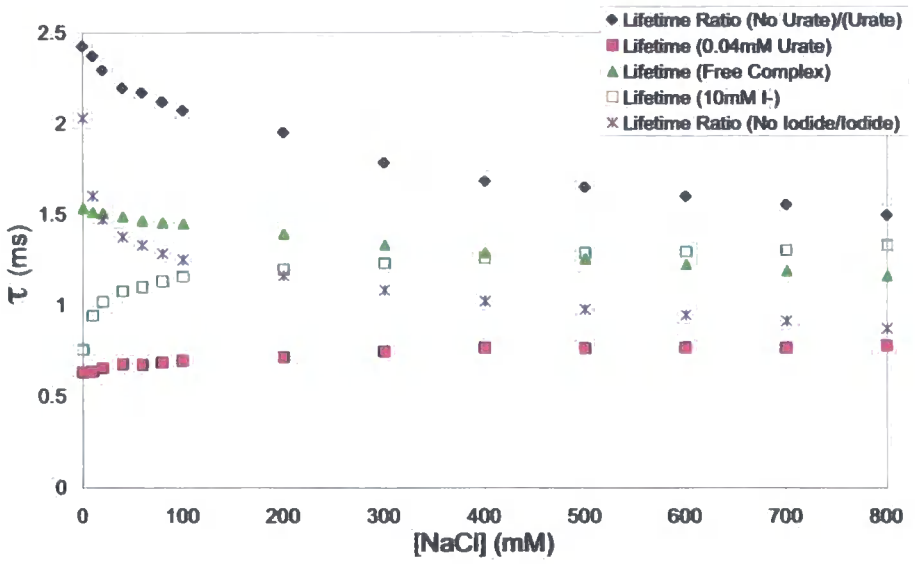

Figure 3.8 Increasing NaCl concentration in the absence and presence of urate and iodide (0.1M HEPES, 10μM $[TbPh_3AzaH]^{3+}$, pH 7.4, 298K)

3.1.4 Catecholate Quenching Studies

Stern-Volmer quenching constants, K_{sv}^{-1} were obtained for a series of catechols which were studied alongside urate and ascorbate, as their oxidation potentials are comparable.

	K_{sv}^{-1} (mM^{-1})	k_q ($M^{-1}s^{-1}$)	τ_0/τ
Ascorbate	0.37	1.2×10^6	1.32 (0.1mM)
Urate	0.03	2.2×10^7	4.48 (0.1mM)
Dopamine	0.17	3.8×10^6	1.59 (0.1mM)
DOPA	0.11	5.9×10^6	1.97 (0.1mM)
3,4-dihydroxyhydrocinnamate	0.05	1.3×10^7	3.26 (0.1mM)

Table 3.2 Values of K_{SV}^{-1} and k_q for the quenching of $[TbPh_3AzaH]^{3+}$ by various oxidants (0.1M HEPES, 10μM $TbPh_3AzaH$, pH 7.4, 298K)

The observed quenching (Table 3.2), by the catechol derivitives examined is comparable to that of urate. This is most apparent for 3,4-dihydroxyhydrocinnamate, which is the only anionic catechol considered. The K_{SV}^{-1} values for the catechols reveal

the effect of quencher charge on the quenching of luminescence. The degree of quenching follows the ordering of charge with [3,4-dihydroxyhydrocinnamate]$^-$ > DOPA > [dopamine]$^+$.

The extent of quenching for the catechols was encouraging, as it was probable that many catechol derivatives could be potentially utilised as intramolecular quenchers for incorporation into a complex. They needed to possess a favourable oxidation potential, an absorbance out of range of that of the chromophore and should preferably be easily attached to the ligand framework.

If the catechols were to be attached to a complex they may need to be protected due to the facility of aerial oxidation in aqueous solution. Quenching studies were performed with the methylene-protected catechols, and even though their oxidation potentials appeared to be unfavourable[6] in non-aqueous media for the electron transfer, 1.50V (0.1M ^{t}Bu$_4$NPF$_6$, MeCN), with this value being relatively similar under aqueous conditions), dynamic quenching was still observed (Table 3.3). The free catechol shows an oxidation potential of 1.41V under these conditions (in their non-ionised form). The complexes [LnPh$_3$AzaH]$^{3+}$ and [LnDO3AdpqC] were both studied, as they demonstrate a difference in chromophore, steric bulk and overall complex charge (Figure 3.9).

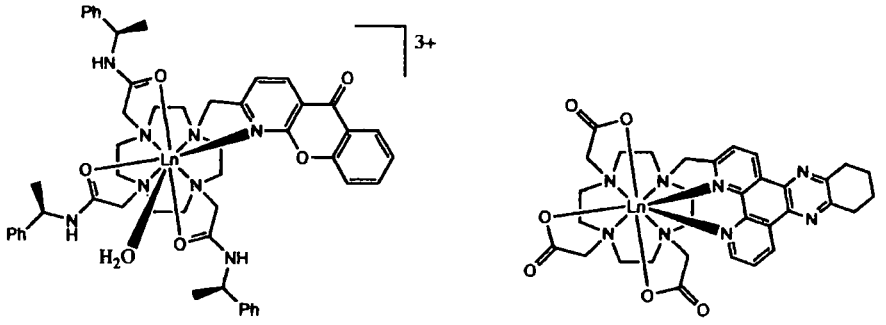

Figure 3.9 [LnPh$_3$AzaH]$^{3+}$ (left) and [LnDO3AdpqC]

K_{sv}^{-1} (mM^{-1})	$[EuPh_3AzaH]^{3+}$	$[TbPh_3AzaH]^{3+}$	[EuDO3AdpqC]	[TbDO3AdpqC]
Ascorbate	1.5	0.37	4.31	0.3
Urate	0.6	0.03	0.04	0.006
3,4-dihydroxyhydro cinnamate	0.06	0.05	0.17	0.06
3,4-(methylenedioxy) phenyl acetic acid	45	1.81	15.5	2.00
3,4methylene-dioxybenzylamine	95	7	-	-

Table 3.3 Values of K_{SV}^{-1} for the quenching of $[LnPh_3AzaH]^{3+}$ and [LnDO3AdpqC] by various oxidants (0.1M HEPES, 10mM NaCl, 10μM Complex, pH 7.4, 298K)

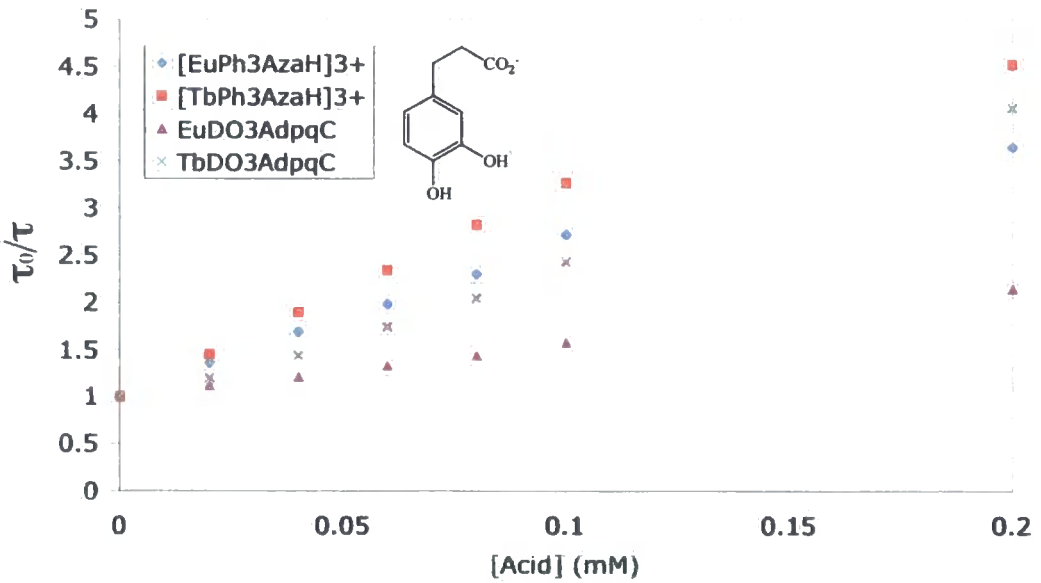

Figure 3.10 Stern–Volmer plot for the quenching of $[LnPh_3AzaH]^{3+}$ and [LnDO3AdpqC] by 3,4-dihydroxyhydrocinnamate (0.1M HEPES, 10μM Complex, 10mM NaCl, pH 7.4, 298K)

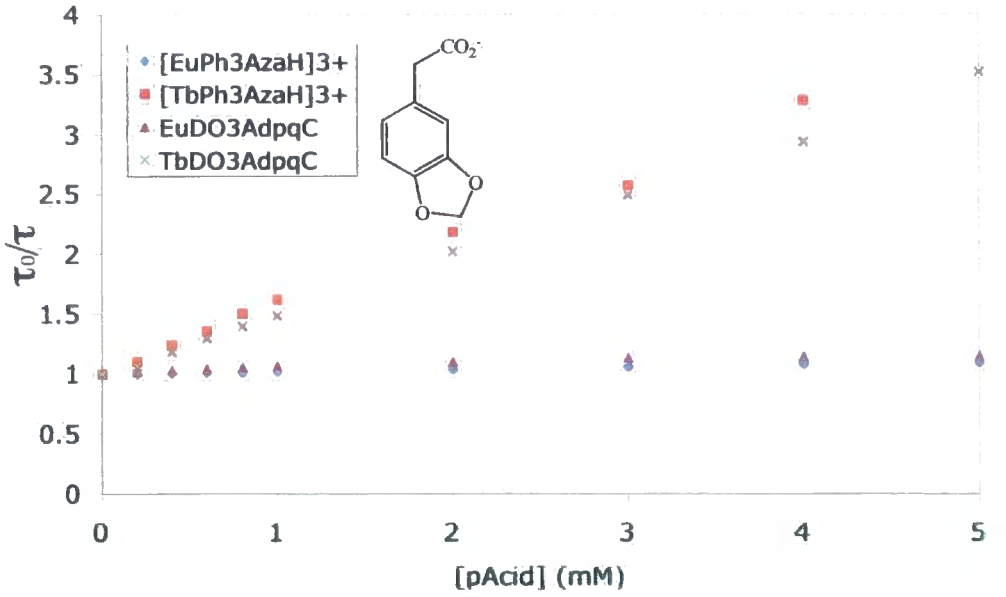

Figure 3.11 Stern–Volmer plot for the quenching of $[LnPh_3AzaH]^{3+}$ and [LnDO3AdpqC] by 3,4-(methylenedioxy)phenyl acetic acid (0.1M HEPES, 10μM Complex, 10mM NaCl, pH 7.4, 298K)

The free catechol is a more powerful reductant, which is reflected in the K_{sv}^{-1} values, which are shown to be very similar for all complexes. The protected catechol shows a more marked difference between europium and terbium complexes, with the terbium complexes being more susceptible to quenching. These results are consistent with the trends previously observed[2] (Figures 3.10 and 3.11).

3.1.5 Encounter Complex / Exciplex Formation

Though many of these results only hold for a given complex, with variation of the lanthanide, steric bulk, overall charge and chromophore influencing interactions, some common features can be gleaned from these and related recent results.[7]

Classical Stern-Volmer quenching behaviour, such as that held at low concentrations and by iodide, assumes the formation of a reversible encounter complex, as proposed by Rehm and Weller.[8] This electron transfer process between the donor and acceptor yields a radical-ion pair, which then dissociates rapidly. Studies reveal urate, ascorbate, and selected catecholates to show non-linear quenching behaviour at higher concentrations. This tendency may be related to the kinetic regime where $k_q[Q] \sim k_{em}$, i.e. where the rate

of quenching approximately equals the rate of decay of the observed emission. Urate and the protected catcholates also show surprisingly high quenching ability on the basis of their one-electron oxidation potentials, with urate quenching also characterised by higher order exponential decay processes. Deviations from an encounter complex model have been observed for the quenching of several organic chromophores, and have been alternatively ascribed to the formation of a relatively long-lived exciplex.[9]

$$\tau_0 / \tau = (1+k_3 \tau_0 K_{ex} [Q]) / (1+K_{ex} [Q])$$

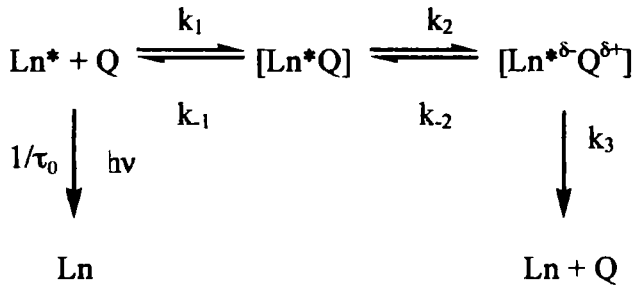

Scheme 3.2 Kinetic scheme for exciplex formation

The above model (Scheme 3.2) involves the formation of a long-lived exciplex rather than radical-ion pairs; the exciplex lifetime is given by $1/k_3$. The equilibrium constant, $K_{ex} \sim k_1k_2/k_{-1}k_{-2}$, provided that $k_{-2} >> k_3$. Therefore, additional factors need to be considered such as the facility of π-stacking between the quencher and the electron poor heterocyclic sensitising moiety as partial charge transfer will contribute more extensively to the modulation lifetime. The apparent Stern-Volmer quenching constant thus becomes a more complex parameter, where the observed lifetime of lanthanide emission may vary non-linearly with increasing quencher concentration. The exciplex model is consistent with the results for quenching by urate, ascorbate and catecholates, in which partial charge transfer occurs between the electron donor and the heterocyclic chromophore of the complex within the lifetime of the excited state of the Ln (III) complex.

Further results confirming this model are explored in two recent publications.[7] Quenching studies with urate, ascorbate and iodide were performed for a family of europium and terbium complexes. Quenching was shown to be sensitive to steric shielding. The addition of protein to the solution led to a very significant suppression of

quenching. Presumably protein binding shields the complex from the interaction with the quenching species. To investigate the complex/quencher interaction further, the solution temperature was varied during irradiation. On increasing the temperature, for both urate and ascorbate addition, the quenching decreased and the emission lifetime increased. This effect may be associated with the exciplex formation being entropically disfavoured. Iodide quenching showed the opposing trend, supporting a classical thermally activated collisional model. These results support the exciplex model for quenching with urate, ascorbate (and also the catecholates), further explaining the poor correlation observed between the redox potentials and the observed quenching sensitivity.

3.2 The 'Quenched' Complex

Each of the complexes synthesised, $[Eu.Q1]^+$ and $[Tb.Q1]^+$, incorporates a protected catechol quencher and a tetraazatriphenylene chromophore, in a *trans* geometry across the cyclen ring system (Figure 3.12). The chromophore, tetraazatriphenylene has been shown to be a highly successful bidentate chromophore possessing low ligand fluorescence, leading to saturated 9-coordinate complexes with high quantum yields and long lifetimes[10]. This chromophore has been extensively studied in relation to quenching[2] and was chosen as the chromophore in preference to an azaxanthone, which is smaller, and only unidentate. The quencher used was a protected catechol, which although possessing a relatively high oxidation potential (1.50V; 0.1M $^nBu_4NPF_6$, MeCN) with respect to urate or ascorbate, has still been shown to quench the excited state of [LnDO3AdpqC], (see Section 3.1.4; pg. 45) with similar Stern-Volmer quenching constants to that of iodide.[2] Studies on these 'quenched' complexes hoped to reveal how attachment of such an entity would affect the luminescence, in comparison to the 'control' complexes [EuDO3AdpqC] and [TbDO3AdpqC].

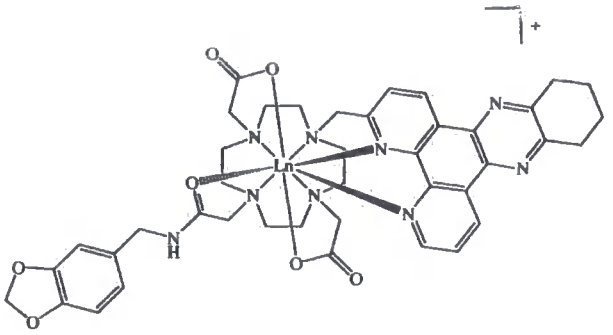

Figure 3.12 Synthesised complex, for both europium and terbium, $[Eu.Q1]^+$ and $[Tb.Q1]^+$

3.2.1 Absorption and Excitation Spectra

The absorption spectra of $[Eu.Q1]^+$ and $[Tb.Q1]^+$, revealed bands associated with each aromatic chromophore, with the 268 nm peak corresponding to both dpqC and catechol absorbance (Figure 3.13). The excitation spectrum confirms that the lanthanide centre can be excited selectively by the dpqC chromophore, with absorbance at 348 nm (Figure 3.13).

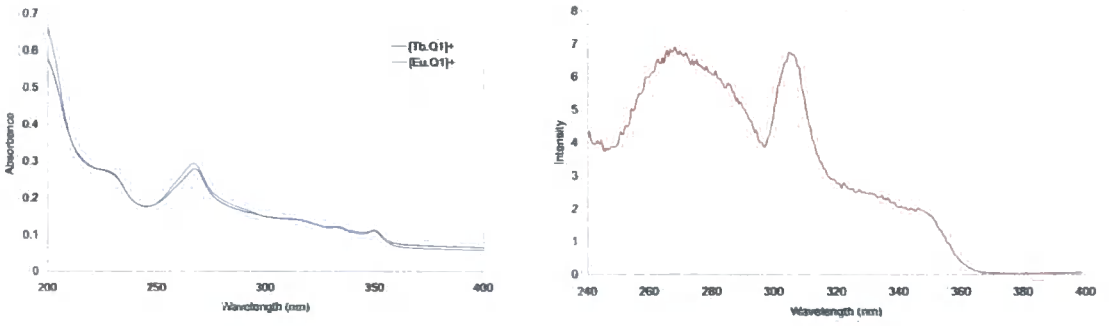

Figure 3.13 Absorption spectra of $[Eu.Q1]^+$ and $[Tb.Q1]^+$, and excitation spectrum of $[Eu.Q1]^+$ (A=0.1, Em=612 nm, 298K). The excitation peak at 306 nm probably corresponds to scattered excitation light being detected.

3.2.2 Emission Spectra

The emission spectra for $[Eu.Q1]^+$ and $[Tb.Q1]^+$ (Figures 3.15 and 3.16), exhibited no chromophore fluorescence due to the minimal fluorescence of dpqC (as a result of its efficient intersystem crossing). The $[Eu.Q1]^+$ emission shows a large $\Delta J=2$ band centred at 615 nm with respect to the $\Delta J=1$ band. This behaviour suggests that the polarisability of the axial donor is low and there is relatively low symmetry about the metal ion. Such

features are to be expected, due to the nature of the coordinating arms. The splitting of the ΔJ=1 transition reveals three components, as expected for the presence of one major solution species.

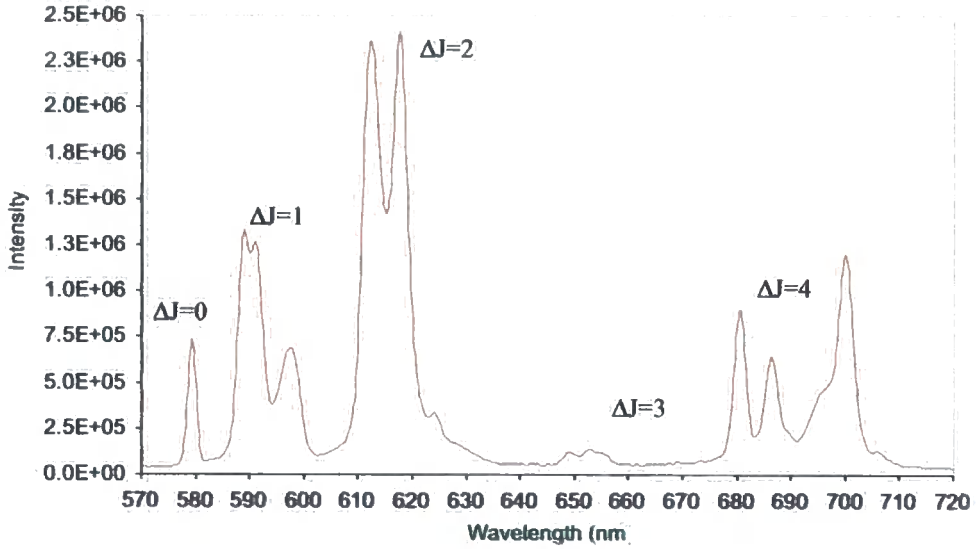

Figure 3.15 Emission Spectrum for [Eu.Q1]$^{+}$ (A=0.1, Ex=348 nm, 298K)

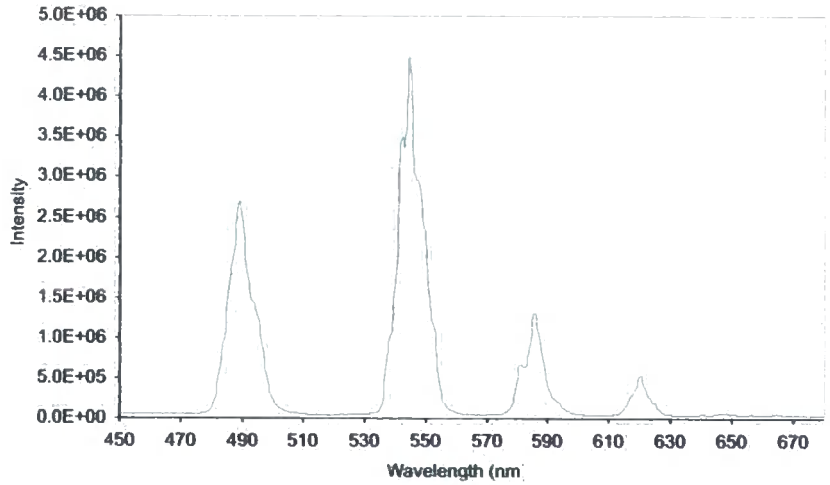

Figure 3.16 Emission Spectrum for [Tb.Q1]$^{+}$ (A=0.1, Ex=348 nm, 298K)

3.2.3 Lifetime and Quantum Yield Measurements

Initial lifetime measurements are consistent with the presence of an effective quenching moiety, within the synthesised complexes (Table 3.4).

	τ_{H2O} (ms)	τ_{D2O} (ms)	k_{H2O} (ms^{-1})	k_{D2O} (ms^{-1})	q
EuDO3AdpqC	1.08	1.67	0.93	0.60	0
TbDO3AdpqC	1.46	1.79	0.68	0.56	0
$[Eu.Q1]^+$	*0.69*	*1.01*	*1.45*	*0.99*	*0.16*
$[Tb.Q1]^+$	0.47	*0.69*	2.13	*1.45*	N/A

Table 3.4 Lifetimes of LnDO3AdpqC and $[Ln.Q1]^+$ in H_2O and D_2O and the corresponding q values. The numbers in italics were recorded on samples prior to HPLC purification. A=0.1, Ex=348 nm, 298 K

The lifetimes are shorter for the synthesised complexes, $[Eu.Q1]^+$ and $[Tb.Q1]^+$ with respect to the previously reported $[LnDO3AdpqC]^2$, with the quenched complex lifetime decreasing by approximately 35% for europium and by 70% for terbium. The $[Tb.Q1]^+$ complex lifetime is reduced more, consistent with observations revealed by the intermolecular quenching studies (see Section 3.1.4; pg. 45).

Lifetime studies on $[Tb.Q1]^+$ revealed a slight curvature in the plot of Ln(intensity) against time for the luminescent decay, implying that there may be more than one decay process occurring. Increasing the concentration of the complex (μM) increased the curvature of these plots with an accompanying lifetime reduction. This behaviour is consistent with the proposal of some degree of intermolecular quenching between neighbouring complexes. The terbium complex also shows a non-linear relationship between integrated emission intensity and absorbance. The non-linearity of the $[Tb.Q1]^+$ decay profile confirms that the calculated value for q, number of bound water molecules is inaccurate, as the equation used (see Section 1.2.6; pg. 23) to calculate q is only valid for a first order and non-competitive decay process. This may also account for the large error present in the $[Eu.Q1]^+$ q value, as there may also be intermolecular

quenching present for this complex, although to a lesser degree. Each complex is very likely to be 9-coordinate, possessing no bound water molecules, as implied by the approximate $[Eu.Q1]^+$ q value of 0.16.

Analytical HPLC was used to probe the purity of the complexes and discover whether there was more than one species present.

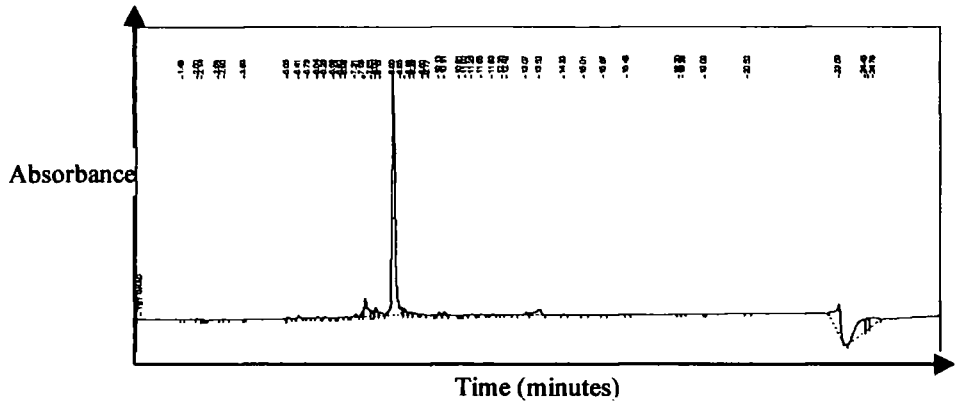

Figure 3.17 HPLC chromatogram of crude $[Tb.Q1]^+$ (absorbance at 254 nm vs. time)

It is evident from the HPLC (Figure 3.17), monitoring absorbance at 254 nm, that 2 species are present. Even though the small peak is <5% of the complex mixture, parallel detection of emission at 546 nm (Figure 3.18) showed it to be highly luminescent. The europium HPLC profile was very similar, but the smaller peak had minimal luminescence.

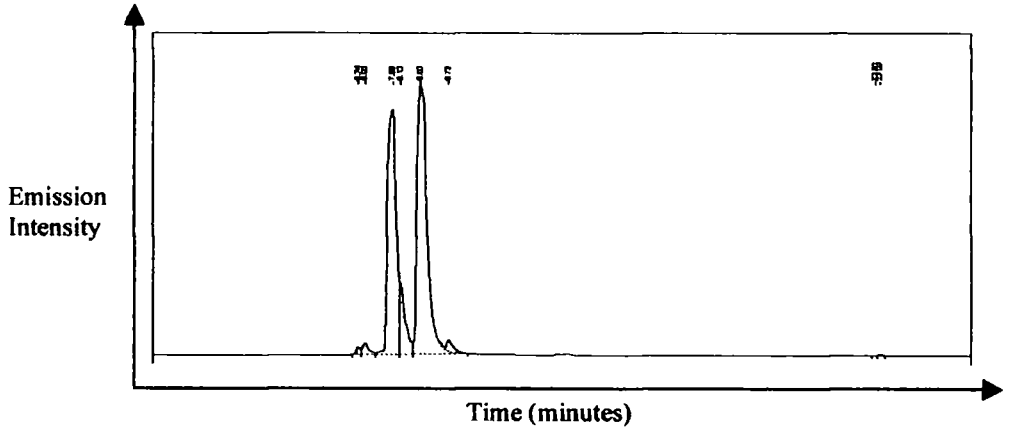

Figure 3.18 Fluorescence chromatogram with detection of emission at 546 nm (relative emission intensity vs. time)

Therefore, preparative HPLC was undertaken to separate the 2 components. But when the complex solution was loaded onto the larger column, a third complex, under the

major peak, was distinguished, which once again though only present in small amounts, was observed to be highly luminescent (Figure 3.19).

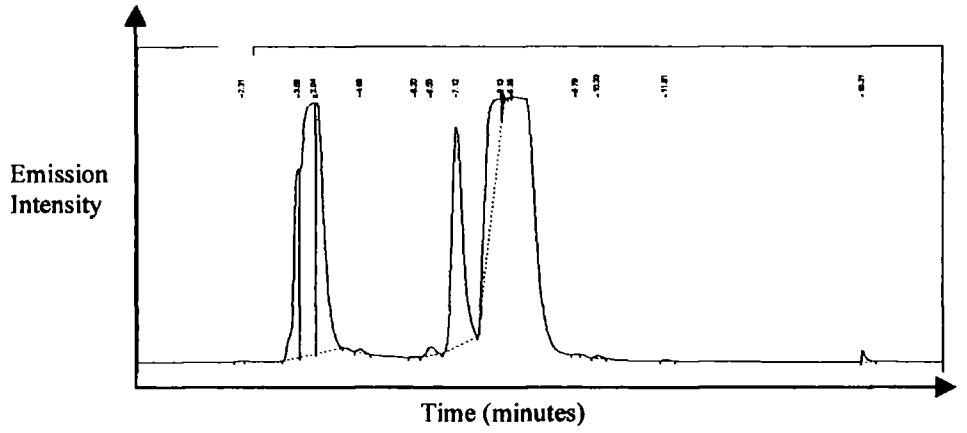

Figure 3.19 Fluorescence chromatogram with detection of emission at 546 nm on preparative column (and different method to separate peaks out further; relative emission vs. time)

The three components were separated out and analysed individually. Each complex showed the presence of the dpqC chromophore due to the absorption at 348 nm. The excitation spectrum for each of these varied, with the 2 complexes with the shortest retention time being the most similar with a major peak at 268 nm, whereas the major complex $[Tb.Q1]^+$ (with the longest retention time) had an excitation spectrum similar to that of $[Eu.Q1]^+$. The lifetime for each of these varied immensely: component 1 had a lifetime of 1.46 ms; component 2 had a lifetime of 2.14 ms. The lifetime of the purified sample of $[Tb.Q1]^+$ was reduced to 0.47 ms, now that it was separated. Although the structure of the two earlier components is still questionable, it is known that each should possesses a dpqC chromophore, from both the excitation and absorption, and the latter must be very structurally similar to $[Tb.Q1]^+$. From ESMS analysis, component 1 shows the presence of both the monosubstituted and disubstituted catechol complexes, although the emission and absorption spectra suggest that dpqC should be present; component 2 looks as though it incorporates the complexes $[TbDO3AdpqC+Na]^+$ and $[TbDO2AdpqC]^+$.

The decay profile (logI vs. time) of the purified $[Tb.Q1]^+$ complex still showed distinctive curvature, which was more pronounced at higher concentrations. Therefore, intermolecular quenching was still probably occurring between the catechol moiety of one complex and the dpqC of another, complicating the luminescent decay profile and resulting in an overall reduction in lifetime at higher concentrations.

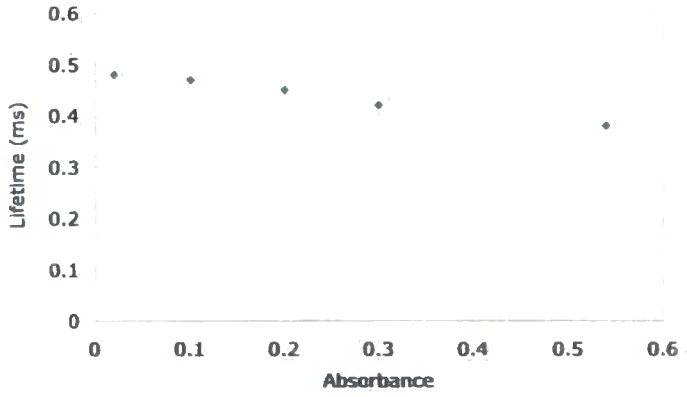

Figure 3.20 Variation of observed emission lifetime with [Tb.Q1]$^+$ concentration

Figure 3.20 displays the change in lifetime with increasing $[Tb.Q1]^+$. The decreasing lifetime is easily related to intermolecular quenching. This mechanism of quenching is not present for $[Eu.Q1]^+$, and if so, only to a small extent. Increasing the concentration of $[Eu.Q1]^+$ to the same degree had no effect on the lifetime, which can be related to the fact that the excited europium ion is less susceptible to quenching. $[Eu.Q1]^+$ also lacks the curvature that $[Tb.Q1]^+$ exhibits, suggesting that the luminescent decay is via one major decay process.

Thus, the lifetime of $[Tb.Q1]^+$ with respect to TbDO3AdpqC is reduced by closer to 70% from 1.46 ms to 0.47 ms. The lifetime of $[Eu.Q1]^+$ will probably not change tremendously from the value of the crude, 0.69 ms as the 2 complexes with the shorter retention time are almost non-luminescent, but separation is necessary before values for quantum yield and lifetime are definitive.

3.2.4 The Two-Electron Photoreduction

The observed curvature of the exponential decay profile for the terbium complex raised the possibility of a chemical reaction occurring during the photoexcitation process. When $[Tb.Q1]^+$ was first synthesised and characterised by ESMS, the complex mass was found to be 934 (100%), with good agreement between observed and calculated isotope patterns (Figure 3.21). On running an ESMS analysis on a previously excited sample, it was found that the observed mass of the complex had increased by 1,2 and 3 units, with the 2-unit change being the dominant species (Figure 3.22). This implies a

reduction process may have occurred with hydrogen abstraction from another species. On running mass spectra for other samples, such as the original sample used for the MS a week previously, it was found that some samples retained the same mass of the original complex, suggesting that this process is photochemically driven and so related to the degree of exposure to UV light and complex concentration, a finding which may also explain the inconsistency in luminescent decay gradients.

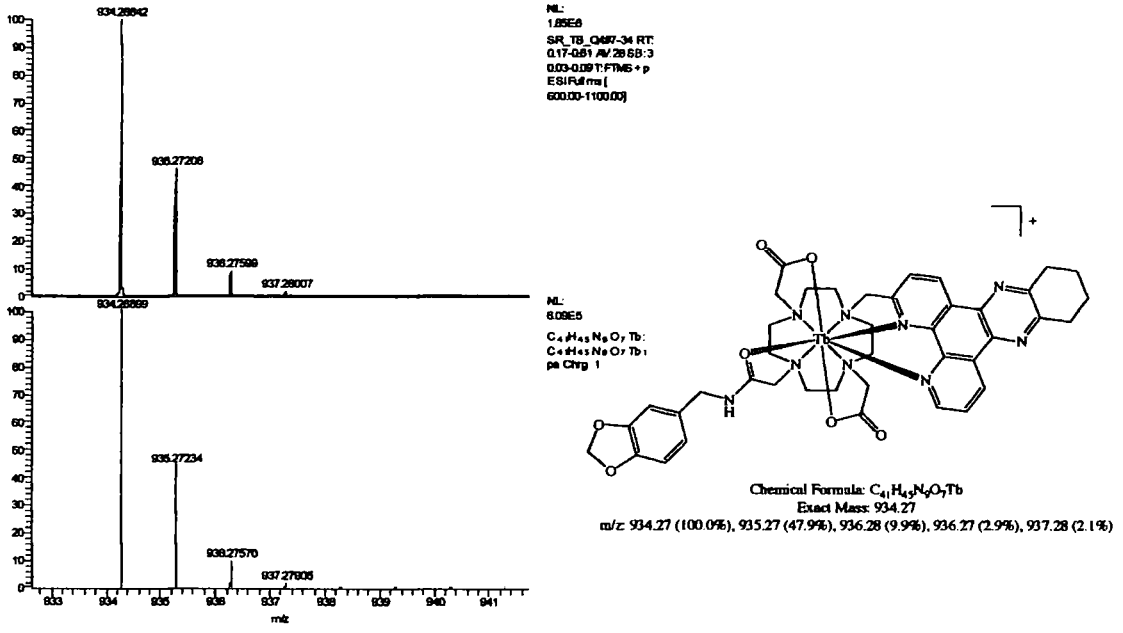

Figure 3.21 Mass spectrum of irradiated [Tb.Q1]$^{+}$ prior to illumination, and (below) the calculated isotope pattern

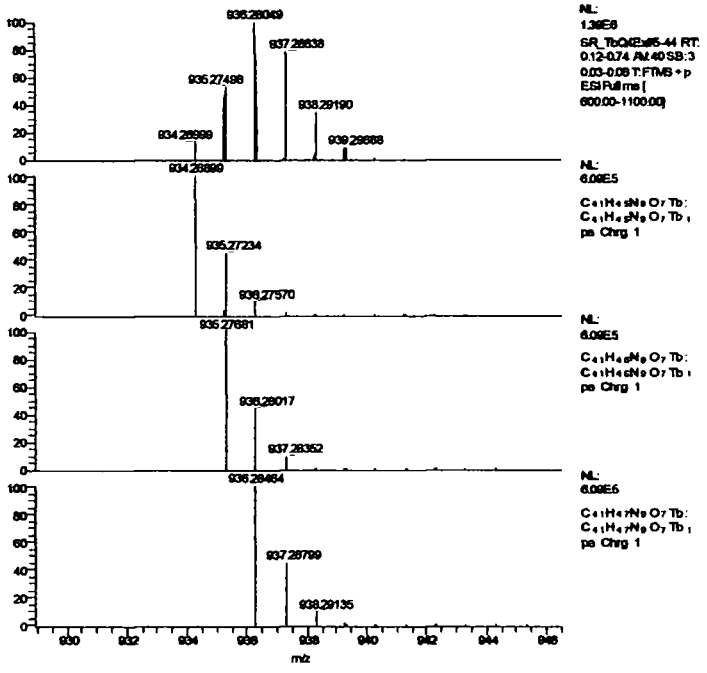

Figure 3.22 Mass spectrum of previously excited $[Tb.Q1]^+$ and predicted fits for $[M+H]^+$ and $[M+2H]^+$. Note that the measured accurate masses will be subject to error due to peak broadening as a result of peak overlap.

It is evident that a chemical reaction is occurring during photoexcitation. This photoexcitation although chemically altering the structure, appears to have no effect on the lifetime of the complex, which remains that of the initial excited sample. Studies on the europium analogue, $[Eu.Q1]^+$, shows that this complex, to date, shows no evidence for mass change as a function of its degree of photoexcitation.

In order to probe the mass change, an experiment was performed in D_2O. The sample used in the original ESMS measurement (that had not been previously excited) retained its mass spectral profile with a single species at 934. Therefore, this sample was washed thrice with D_2O and photoexcited for one hour in D_2O under argon using a tungsten lamp. The D_2O was then removed and the sample washed with H_2O three times. ESMS analysis was then undertaken on the sample.

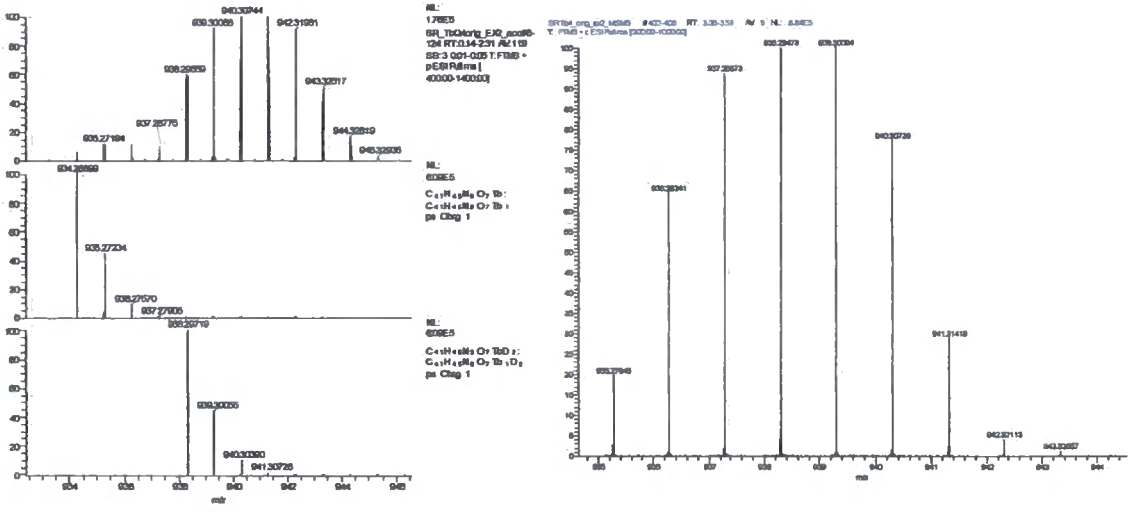

a) *b)*

Figure 3.23 Mass spectra after D_2O exchange and then photoexcitation; a) the spectrum on the left is the initial ESMS with the [M+4] isotope model below; b) the spectrum on the right is the same ESMS but after the sample was left in MeOH/H_2O for 1 week (to allow complete exchange of exchangeable hydrogens and/or aerial oxidation/rearomatisation)

A mass increase of $[M+2H]^+$, $[M+4H]^+$, $[M+6H]^+$ was observed (Figure 3.23b), instead of the previous $[M+H]^+$, $[M+2H]^+$, $[M+3H]^+$, due to non-exchangeable deuterium transfer occurring upon photoexcitation. The mass spectrum obtained also showed an extended range of peaks, including those predicted from the doubling of the hydrogen mass, but also further species. The experiment confirmed that there is a chemical alteration occurring upon photoexcitation, involving irreversible hydrogen abstraction from water. This reduction/hydrogen abstraction is unusual, as the oxidation potential of water is low and therefore an unlikely oxidant. The complex reduction could either be occurring on the catechol moiety or dpqC, each of which would result in the same mass change (Figure 3.24).

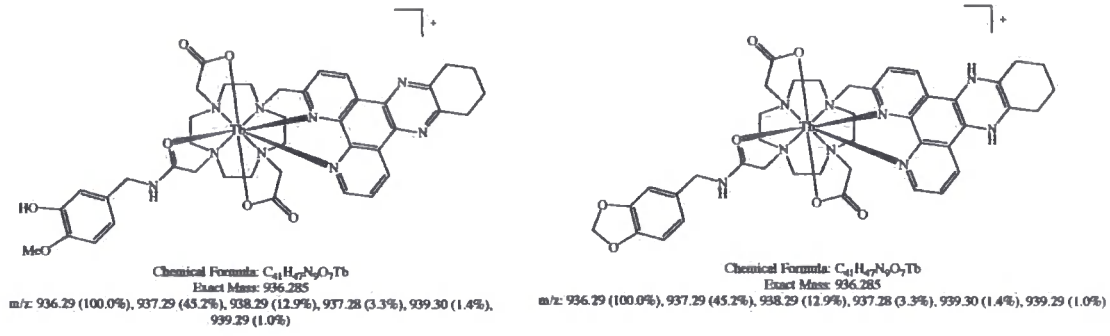

Figure 3.24 Putative products formed upon photoexcitation of $[Tb.Q1]^+$, involving a mass change from 934 to 936

Either the catechol undergoes reductive ring cleavage or the dpqC chromophore is reduced. The absorption spectral profile of the 'reduced' sample was invariant with pH over the range 5 to 11. An MSMS experiment was performed to probe whether fragmentation would reveal the site of reduction. Distinctive fragmentation peaks of 713 and 649 were ascribed to the following species (Figure 3.25).

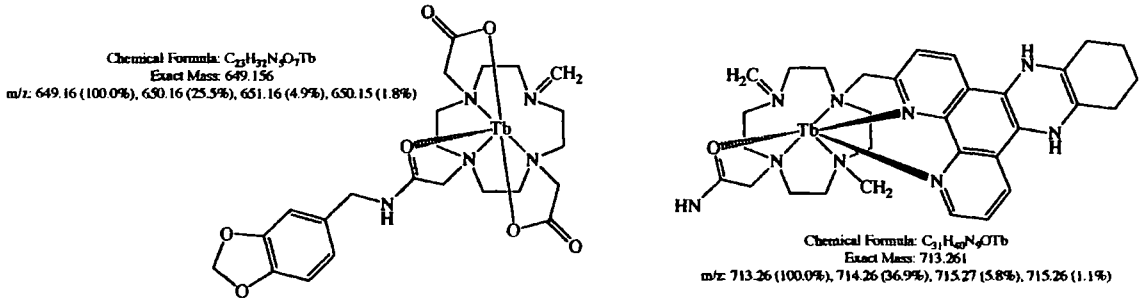

Figure 3.25 Chemical species formed by MSMS on the photoexcited sample, involving cleavage of the $[Tb.Q1]^+$ complex

Thus, the fragmentation revealed that it was in fact the bipyridyl ring that was undergoing the reduction, confirmed by these 2 distinctive fragmentation peaks. This was further confirmed by MSMS analysis of the deuterated sample, where the 713 mass peak became 715, due to the unexchangable deuteration of the ring system.

The mass change of 1,2, and 3 Daltons can explained by the different extent of reduction, which when reaching an equilibrium, may lead to the formation of a species with a mass of 936 as the major component, involving the protonation of the 2 pyrazine ring nitrogens. As the conjugation of the dpqC system is only slightly perturbed, this explains the consistency of the photophysical measurements, notwithstanding the duration of sample excitation (Figure 3.26).

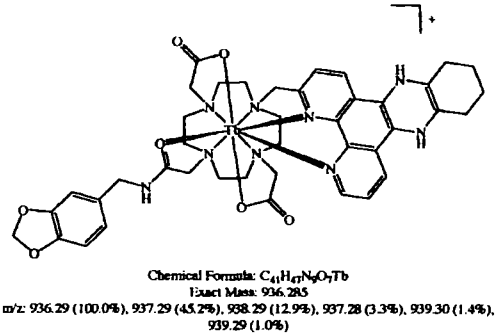

Figure 3.26 Hypothetical product of the photoreduction of $[Tb.Q1]^+$ during excitation in H_2O (λ_{em}=348 nm)

In order to rationalise the formation of isotopomers with a mass of >2 or 4 units in the D_2O experiment, then exchange of H or D at CH bonds must be occurring. Therefore the observed profile must be due to [reduction (+2) + CH/CD], thus the aromatic system undergoes significant exchange. This is plausible if charge builds up at both N and C, (Figure 3.27), consistent with the resonance forms depicted below.

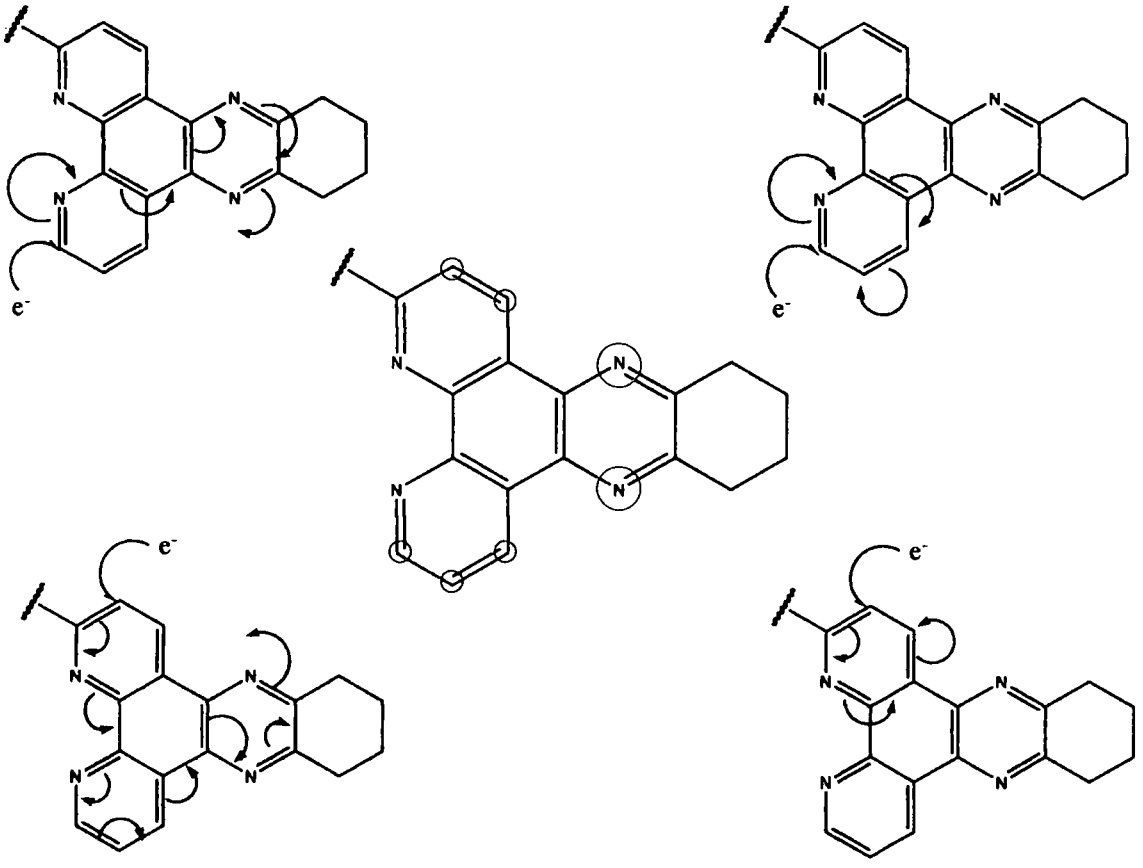

Figure 3.27 Variation of charge localisation around the dpqC ring system, with the most feasible sites for H/D exchange highlighted

The photoreduction of the related ligand, dppz, in alcohols, has been reported by Kelly[11] (Figure 3.28);

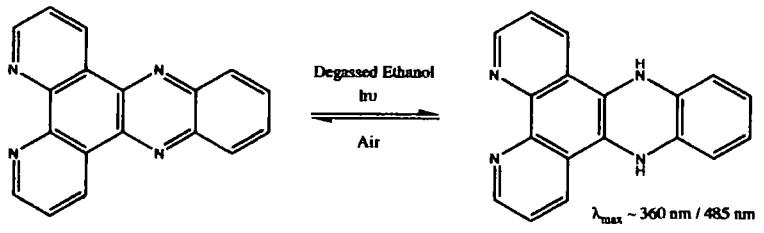

Figure 3.28 Reduction of dppz by photoexcitation in degassed ethanol

The dppz system differs in that it is more extensively conjugated which may account for the reversibility of the reaction; re-aromatisation occurs readily in the presence of air. The reaction occurred rapidly in 2-propanol but was slower in methanol, in accordance with the ease of abstraction of the hydrogen. Kelly proposed, with the aid of density functional theory calculations, that the dppz triplet state extracts a hydrogen atom from the ethanol forming a radical species, dppzH$^{\cdot}$ (1), which then disproportionates (2). This mechanism is similar to that proposed for the photoreduction of phenazine and related compounds.

$$^3\text{dppz}^* + R_2CHOH \rightarrow \text{dppzH}^{\cdot} + R_2C^{\cdot}OH \quad (1)$$

$$2\text{dppzH}^{\cdot} \rightarrow \text{dppzH}_2 + \text{dppz} \quad (2)$$

On studying this photoreduction in the presence of rhenium, in the form of $[Re(CO)_3(dppz)(py)]Cl$ (py=pyridine), it was found that the forward reduction step occurred readily, though the reverse re-aromatisation reaction was 'significantly slower'.

These results suggest that in the case of the $[Tb.Q1]^+$ photoreduction, the re-aromatisation must be a slow process that is prolonged by the presence of the metal ion (Tb^{3+}).

The reduced complex was left stirring overnight in the presence of MnO_2 to determine whether the complex could be oxidised back to the original form. The isotope pattern changed and a new series of peaks appeared throughout the spectrum, lowering the signal in the region of the singly charged complex. It did appear that the tetraazatriphenylene moiety could be oxidised back to its original form, but some competitive decomposition reactions were also occurring.

The original oxidised complex was stirred overnight in $NaBH_4$ to determine whether the reduction could be driven chemically instead of photolytically; no change was observed suggesting that the interaction is one between the quencher and the tetraazatriphenylene chromophore, with exposure to high intensity light required to drive the electron transfer reaction.

3.2.5 Photoexcitation of Analogous Complexes

Further investigations were performed on the analogous terbium complexes, [TbDO3AdpqC] and $[TbPh_3dpqC]^{3+}$.

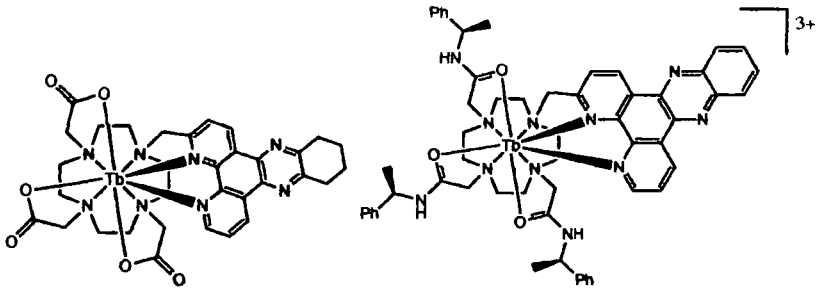

Figure 3.29 Structures of [TbDO3AdpqC] and $[TbPh_3dpqC]^{3+}$

The above complexes did not show the distinct curvature of the exponential decay that was seen for $[Tb.Q1]^+$, implying no other quantitative decay processes were present. To verify the stability of these complexes with respect to light, they were exposed to tungsten light excitation in a range of conditions; varying the exposure time, solvent and presence of quenching moiety.

No change in ESMS was seen for either complex in H_2O, MeOH and D_2O after exposure to the lamp for 1-6 hours. This suggested that no chemical change was taking place. Therefore, the intramolecular quencher was necessary for the reduction process and in its absence the tetraazatriphenylene chromophore was stable to chemical transformation.

The complexes were then excited in the presence of added quencher. Urate and the protected catechol were added to the complex solutions in H_2O, using ten-fold excess of quencher. After exposure, the complexes appeared to have a more complex mass spectra implying the complexes decompose under such conditions.

These results confirm that although the exciplex may be a relatively long-lived state, it has a short lifetime with respect to that of the 2-electron photoreduction. In the case of the intermolecular quenching process, the lifetime of the exciplex is long enough for

deactivation of the excited lanthanide state but too short for the electron transfer process to occur to tetraazatriphenylene. Whereas, the intramolecular quenching for $[TbQ1]^+$, in which the quenching moiety and tetraazatriphenylene are held in close proximity, results in deactivation of the lanthanide excited state as well as the photochemical reduction of the tetraazatriphenylene moiety.

References

[1] a) S. Steenken and P. Neta, *J. Phys. Chem.*, 1979, **83**, 1134; b) S. Steenken and P. Neta, *J. Phys. Chem.*, 1982, **86**, 3661; c) G. R. Buettner, *Arch. Biochem.Biophy.*, 1993, **300**, 535; d) M. G. Simic and S. V. Jovanovic, *J. Am. Chem. Soc.*, 1989, **111**, 5778

[2] a) R. A. Poole, *Luminescent Lanthanide Complexes for Cellular Applications*, PhD Thesis, University of Durham, 2006; b) R. A. Poole, F. Kielar, S. L. Richardson, P. A. Stenson, D. Parker, *Chem. Commun.*, 2006, 4084

[3] J. R. Lakowicz, in *Principles of Fluorescence Spectroscopy*, Kluwer Academic/Plenum Publishers, 1999, 2nd Ed., p. 237

[4] 4th year report, S. L. Richardson, University of Durham, 2006

[5] M. J. Pilling, in *Reaction Kinetics*, Oxford University Press, 1975, p.80

[6] A. Weller, *Pure Appl. Chem.*, 1968, **16**, 115

[7] a) R. A. Poole, C. Montgomery, E. J. New, D. Parker and A. Congreve, *Org. Biomol. Chem.*, 2007, **5**, 2055; b) F. Kielar, C. P. Montgomery, E. J. New, D. Parker, R. A. Poole, S. L. Richardson and P. A. Stenson, *Org. Biomol. Chem.*, 2007, **5**, 2975

[8] a) D. Rehm and A. Weller, *Ber. Bunsenges Phys. Chem.*, 1969, **73**, 834; b) D. Rehn and A. Weller, *Isr. J. Chem.*, 1970, **8**, 259

[9] M. G. Kuzmin, *Pure Appl. Chem.*, 1993, **65**, 1653

[10] R. A. Poole, G. Bobba, M. J. Cann, J-C. Frias, D. Parker and R. D. Peacock, *Org. Biomol. Chem.*, 2005, **3**, 1013

[11] D. A. McGovern, A. Selmi, J. E. O'Brien, J. M. Kelly and C. Long, *Chem. Commun.*, 2005, 1402

4. Conclusions

4.1 Conclusion

The development of responsive ratiometric probes for redox active compounds such as reactive oxygen species, involves an appreciation of the reactivity of the lanthanide emissive state. The lanthanide emissive state can be quenched by vibrational energy transfer to oscillators of appropriate energy, or by electron/charge transfer. The electron/charge transfer from electron rich donors to the chromophore results in 'quenching' of luminescence, where both the emissive intensity and lifetime are reduced as a function of the 'quenching ability' of the oxidant, and the 'susceptibility' of the complex to this electron transfer. Previous work undertaken at Durham had illustrated some common trends which are to be expected; such as the influence of charge, steric bulk and chromophore reduction potential on the Stern-Volmer quenching constant. But some additional trends were also observed; that the oxidation potential pecking order doesn't necessarily dictate the quenching ability; and the influence of the excited state energy of the lanthanide centre to the degree of quenching. Terbium (III) complexes ($^5D_4$ = 2.44 V) were more susceptible to quenching than the europium (III) analogues ($^5D_0$ = 2.06 V), as a result of the higher free energy of the excited state. This difference in sensitivity is a valuable tool in the development of ratiometric probes.

The quenching of luminescence by electron rich donors was further studied in an attempt to derive a mechanism for the quenching process; a mechanism that would take into account all experimental observations. Additional studies were performed on urate, ascorbate and series of catechols; involving ionic strength variation and extended range Stern-Volmer plots. The change in gradients observed for the plots confirmed that the kinetics for the 'quenching' were more complex than a simple kinetic model associated with the formation of a transient 'encounter complex'. As a result of these and further studies, an alternative model was proposed for the quenching process, based upon the formation of an 'exciplex'.

The difference in susceptibility of europium (III) and terbium (III) complexes to quenching affords a promising basis for the development of a ratiometric probe. Thus, the incorporation of a quenching moiety into a complex was proposed to echo the above

trends in an intramolecular manner. The quenching moiety could be various electron rich species, if possessing a suitable oxidation potential. In the proposal to synthesise complexes incorporating a quenching moiety, two complexes have been synthesised, $[Eu.Q1]^+$ and $[Tb.Q1]^+$. These complexes incorporated a tetraazatriphenylene chromophore and a methylene protected catechol positioned *trans* in the cyclen ring system. The initial attempts, to integrate a uric acid derivative was complicated by its insolubility; therefore a methylene protected catechol moiety was used. Lifetime studies on $[Eu.Q1]^+$ and $[Tb.Q1]^+$, showed a reduction of 35% for $[Eu.Q1]^+$ (from 1.08 ms to 0.69 ms), and 70% for $[Tb.Q1]^+$ (1.46 ms to 0.47 ms) with respect to the analogous complexes [EuDO3AdpqC] and [TbDO3AdpqC]. This lifetime reduction is in accordance with the susceptibility of the lanthanide ion to the quenching moiety.

A two-electron photoreduction was also unexpectedly observed for $[Tb.Q1]^+$, where the bipyridyl ring undergoes reduction, confirmed by solvent isotope and MSMS studies.

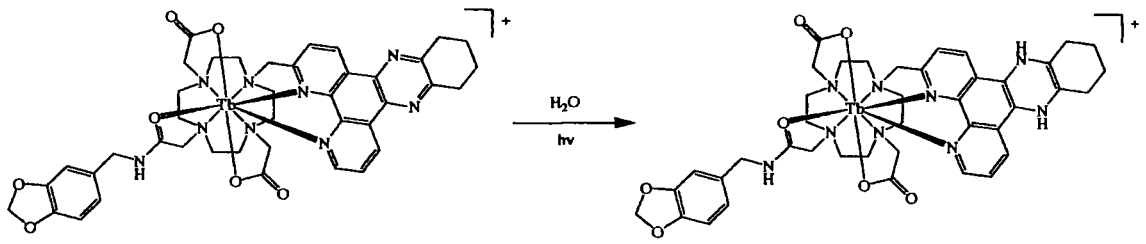

4.2 Further Work

A series of further experiments may now be considered in seeking to extend the research described. They are listed below, according to the stated aspect.

4.2.1 The Two-Electron Photoreduction

i) Attempt to induce the photoreduction of $[Eu.Q1]^+$ under prolonged/harsher conditions in both H_2O and D_2O

ii) Attempt the photoreduction of other 'quenched' complexes incorporating the dpqC chromophore

4.2.2 Further Synthesis

i) Work should be initiated on the synthesis of an analogous complex where the dpqC chromophore and the quenching moiety are positioned cis to one another on the cyclen ring system. Completion of this synthesis may demonstrate the relative distance dependence of the quenching.

ii) Vary key structural features such as chromophore, coordinating arms, and linker length of the quenching moiety.

iii) Incorporate a quenching moiety which could potentially reduce the lifetime to a greater extent (although care must be taken to not quench luminescence entirely). A catecholate with one alcohol group protected in the form of a methoxy group should enhance the quenching ability but the catechol would still be stable with respect to oxidation in solution as only one alcohol group is free, therefore resisting the ring opening.

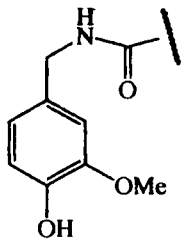

iv) Vitamin E analogues are possible quenching moieties that could be incorporated into a complex. Vitamin E analogues such as Trolox[1] form stable radical species, which can be repaired by ascorbate. A stable radical species could be of major importance, especially in attempting to identify hydroxyl radicals.

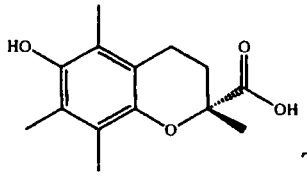

Trolox

4.2.3 Reactive Oxygen Species

These complexes are eventually to be considered for assessment as ratiometric probes, involving permutation of the Ln^{3+} ion, for redox-active species such as ROS. When the complex comes into contact with reactive oxygen species, it should act as an 'off/on' switch, as the extent of quenching by the electron donor should be reduced by preferential electron transfer with the ROS, thereby increasing complex luminescence (Figure 4.1).

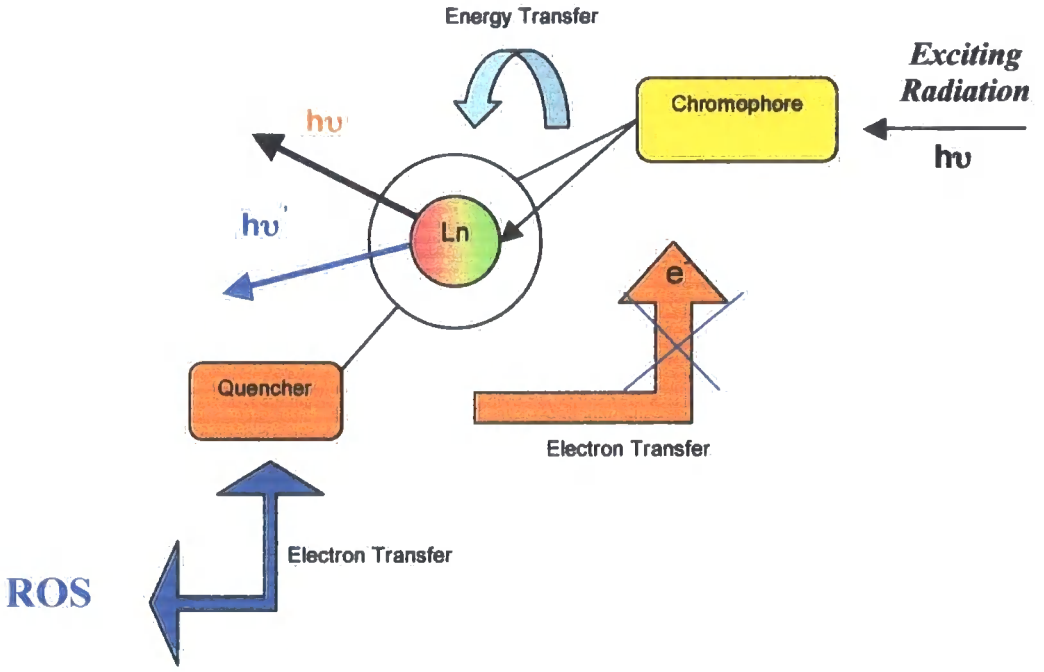

Figure 4.1 Schematic representation of a 'quenched' complex and the potential electron transfer occurring in the presence of ROS, resulting in increased luminescence

It is important that the quenching moiety is able to interact with ROS, thus relaying the effect to the luminescence of the complex, which will provide a probe to relative ROS concentration. This should also be a reversible process. When a more powerful reductant such as ascorbate is added, the luminescence intensity should again decrease back to the 'quenched' value. As it has been demonstrated that complexes of Eu^{3+} and Tb^{3+} respond to the incorporated quencher to different degrees, upon interaction with ROS this should relay a ratiometric measurement in response to ROS concentration.

i) Once the complexes have been purified via HPLC, preliminary tests with ROS should be performed, initially with H_2O_2, as it is the most accessible and stable of the ROS. Lifetime and emissive studies will exemplify the direction of study; as if the complexes show little or no effect in terms of luminescence then modification of complex structure must be undertaken.

ii) Perform a control experiment in which the quenching of the synthesised complexes $[Eu.Q1]^+$ and $[Tb.Q1]^+$ is studied, in the presence of the powerful reductant ascorbate. Whether the complex shows susceptibility to ascorbate and to what extent would help to clarify the effect of the internal quencher.

4.2.4 Exciplex Model

Following direct excitation of the lanthanide centre, e.g. using a 488 nm argon ion laser for terbium, the lanthanide will be promoted to its emissive state, with the chromophore remaining in its ground state. On addition of a quenching species, if the lifetime/emission properties of the complex is reduced, it would confirm that the exciplex formation/electron transfer occurs whilst the chromophore is in its ground state, whereas, if there is no effect of the quencher on the lanthanide emissive properties, it supports the involvement of the chromophore excited state in the quenching process.

References

[1] V. J. Forrest, Y. H. Kang, D. E. McClain, D. H. Robinson and N. Ramakrishnan, *Free Radical Biol. Med.*, 1994, **16**, 675

5. Experimental

5.1 General Experimental and Measurements

Reactions requiring anhydrous conditions were performed using Schlenk-line techniques under an atmosphere of dry argon. All commercially available reagents were used as received, from their respective suppliers. Solvents were dried using an appropriate drying agent when required. Water was purified by the 'Purite$_{STILL}$ plus' system.

Thin layer chromatography was carried out on neutral alumina plates (Merck Art 5550) or silica plates (Merck 5554), which were visualised under UV (254 nm) or by staining with iodine. Preparative column chromatography was performed using neutral alumina (Merck Aluminium Oxide 90, activity II-III, 70-230 mesh), pre-soaked in ethyl acetate, or silica (Merck Silica Gel 60, 230 ± 400 mesh).

^{1}H and ^{13}C were recorded on a Varian Mercury 200 (^{1}H at 199.975 MHz, ^{13}C at 50.289 MHz), Varian Unity 300 (^{1}H at 299.908 MHz, ^{13}C at 75.412 MHz), Varian VXR 400 (^{1}H at 399.968 MHz, ^{13}C at 100.572 MHz), or a Bruker AMX 500 spectrometer. Spectra were referred internally to the residual protio-solvent resonances and are reported relative to TMS. All chemical shifts are quoted in ppm and coupling constants in Hz. Splitting patterns are described as singlet (s), doublet (d), triplet (t), or multiplet (m). Electrospray mass spectra were recorded on a VG Platform II (Fisons instrument), operating in positive or negative ion mode as stated, with methanol as the carrier solvent. Accurate mass spectra were recorded using a Thermo Finnigan LTQ FT mass spectrometer. Melting points were recorded using a Köfler block and are uncorrected. UVVis absorbance spectra were recorded on a Perkin Elmer Lambda 900 UV/Vis/NIR spectrometer. Emission Spectra and Lifetimes were measured on a Fluorolog-3 and a Perkin Elmer LS55 luminescence spectrometer using FL Winlab software. All samples were contained in quartz cuvettes with a path length of 1 cm and measurements obtained relative to a reference of pure solvent contained in a matched cell. Emissive studies were performed using excitation and emission slit widths of 10 and 2.5 nm respectively. Slit widths were consistent through all measurements unless otherwise stated.

The quantum yield is defined as the number of photons emitted divided by the number of photons absorbed. An absolute quantum yield cannot be measured due to lack of techniques and equipment; therefore the quantum yield is measured relative to the known quantum yield of a 'standard' complex.

$$\phi_x = \phi_r . (A_r / A_x).(E_x/E_r).(I_r /I_x).(n^2_x/n^2_r)$$

A = absorbance at excitation wavelength
E = corrected integrated emission intensity
I = corrected intensity of excitation light (same conditions used throughout)
n = refractive index of solution
r and x refer to the reference and unknown respectively.

All the measurements were made relative to $LnPh_3dpqC$ ($Ln=Eu^{3+}$ or Tb^{3+}). The absorbance at the excitation wavelength and the total integrated emission were recorded for 6 samples between 0.02 and 0.2 absorbance for the Eu and Tb complexes. A graph of integrated emission against absorbance gave a linear plot, and substitution of the gradient into the following equation (cancelling refractive indexes) determined the quantum yield relative to the standard.

$$\phi_x = \phi_r . (gradient_x /gradient_r).(n^2_x / n^2_r)$$

The quantum yield measurements contain an error of ±10%. Errors arose from the inner filter effect, and amount of absorbed light. These errors were minimised by using samples with < 0.2 absorbance and using a small excitation band pass width.

The lifetimes of the europium and terbium complexes were measured by exciting the sample with a short pulse of light (348 nm in the case of dpqC complexes) and monitoring the integrated intensity of light (546 nm for Tb and 612 nm for Eu) emitted from the sample. Emission was recorded during a fixed gate time, t_g (0.1 ms), and delay time, t_d, which is the time taken for the intensity to decay to half of its original value upon excitation. At least 20 delay times were measured, covering 3 or more lifetimes. The obtained decay curves were fitted to the equation below using Microsoft Excel.

$$I(t) = I_0 \exp(-kt)$$

I(t) = intensity at time, t, after excitation

I_0 = initial intensity at time, t=0

k = rate constant for decay of excited state

The inner sphere hydration of the complexes was calculated via the rate constants, using the lifetimes for the complexes in H_2O and D_2O.

$$k_{H2O} = k_{nat} + k_{nr} + \sum k_{XH} + \sum k_{C=O}$$

$$k_{D2O} = k_{nat} + k_{nr} + \sum k_{C=O}$$

k_{nat} = natural radiative constant

k_{nr} = non-radiative deactivation

$\sum k_{XH} + \sum k_{C=O}$ = sum of energy transfer to close proximity oscillators

In D_2O there is no contribution from XH oscillators therefore the difference in the rate constants for H_2O and D_2O gives $\sum k_{XH}$ for the complex. Assuming the predominance of OH quenching in aqueous media, an approximation for the number of bound water molecules can be made. Corrections are made for each of the lanthanide ions: a proportionality constant reflecting the sensitivity of each of the lanthanide ions to vibronic quenching by OH oscillators, and a correction terms for the presence of closely diffusing OH oscillators. For Eu, a further correction of 0.08 ms^{-1} was made for the presence of the proximate amide NH oscillator.

$$q_{Eu} = 1.2\,[(k_{H2O} - k_{D2O}) - 0.25]$$

$$q_{Tb} = 5\,[(k_{H2O} - k_{D2O}) - 0.06]$$

(Where 1.2 and 5 have the units of milliseconds)

For the quenching studies, the change in emissive lifetime of the complexes was measured in the presence of varying quencher concentration. The quenching species studied were ascorbate, urate, and a series of catechols. Emission and excitation slit widths of 10 nm were used. Standard complex solutions of 10 μM complex were used, containing 10 mM NaCl, with buffering of the solution to pH 7.4 with Hepes (100 mM).

Various quenching concentrations were used, measuring the absorbance and emissive decay in each case. Plots of τ_0/τ against quencher concentration [Q] were used to determine the Stern-Volmer quenching constant, K_{SV}^{-1} as the gradient. Control experiments examining the variation of emission intensity, I_0/I against [Q] showed the same behaviour consistent with a dynamic quenching process.

Reverse phase HPLC were performed at 298 K on a Perkin Elmer system using a 150 x 4.6 mm Phenomenex Synergi 4μ Fusion-RP 80 column. A H_2O + 0.1% formic acid / CH_3CN + 0.1% formic acid solvent system was used (gradient elution). Gradient programme:

Time (min)	H_2O + 0.1% formic Acid (%)	CH_3CN + 0.1% formic Acid (%)	Gradient
0	100	0	0
15	0	100	1
20	0	100	0
25	100	0	-3
27	100	0	0

5.2 Experimental Procedures

5.2.1 Uric Acid Derivitives

2,6,8-Trichloropurine[1]

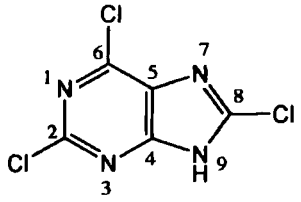

Uric acid (10.0 g, 59 mmol) was dissolved in phosphoryl chloride (50 ml, 546 mmol) and dimethylaniline (22.4 ml, 177 mmol) forming a cloudy yellow solution. The solution was refluxed at 130 °C with the exclusion of water, resulting a cloudy green solution. After 18 hours the dark green solution was cooled and half the solvent removed under reduced pressure. The remaining solution was poured onto crushed ice

(150 g) forming a light brown solution – after time a dark brown suspension was formed. The solid was filtered and washed with diethyl ether. The aqueous filtrate was then washed with diethyl ether (3 x 100 ml) and the ether washings combined (including those from the precipitate washings). The ether was removed under reduced pressure yielding an orange solid. The orange solid was then dissolved in boiling 3M ammonia solution and the hot solution was filtered. As the ammonia solution cooled the product quickly precipitated out of solution as the ammonium salt. The pale yellow solid was collected, washing with water, and was then dissolved in 75 parts of boiling water forming a yellow solution which was acidified to pH 2 via addition of sulphuric acid and filtered hot over a filter agent. On the cooling the product precipitated out of the aqueous solution and was collected via centrifuging, drying under reduced pressure yielded a pale yellow solid (3.2 g, 14 mmol, 24%), m.p. 176-178 °C (lit. 185 °C). R_f=0 (40:60 ethyl acetate:hexane). Found: C, 25.52; H, 0.72; N, 23.88. $C_5HCl_3N_4.1/2H_2O$ requires C, 25.83; H, 0.87; N, 24.11. The insolubility of the product precluded solution-state NMR analysis.

7- and 9-(tert-Butoxycarbonylmethyl)-2,6,8-trichloropurine[2]

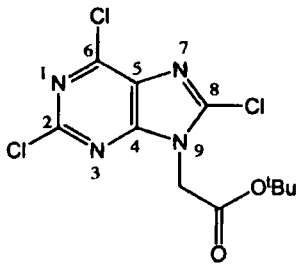

Trichloropurine (250 mg, 1.12 mmol), ^{t}butyl bromoacetate (0.17 ml, 1.12 mmol) and sodium bicarbonate (94 mg, 1.12 mmol) were dissolved in acetonitrile (5ml). The cloudy yellow solution was stirred under argon at 45°C. The reaction was stopped when unwanted products began to form via TLC. The solvent was removed under reduced pressure and the crude product purified by column chromatography (silica, hexane → 20% ethyl acetate:hexane), to give 2 isomers, as white solids.

7-(tert-Butoxycarbonylmethyl) trichloropurine (220 mg, 0.65 mmol, 58%), m.p. 146-148 °C. R_f = 0.72 (40:60 ethyl acetate:hexane). δ_H ($CDCl_3$) 1.46 (9H, s, ^{t}Bu), 5.13 (2H, s, CH_2); δ_C ($CDCl_3$, 125MHz) 28.2 (^{t}Bu), 47.9 (CH_2), 85.1 (^{t}Bu), 123.4 (C^5), 142.8 (C^4),

150.7 (C^8), 154.0 (C^2), 161.5 (C^6), 164.8 ($CO_2{}^tBu$); *m/z* (ESMS$^+$) 337.0 (M *(^{35}Cl)* + H, 100%), 339 (M + H, 90%), 341 (M + H, 30%)

9-(tert-Butoxycarbonylmethyl) trichloropurine (40 mg, 0.12 mmol, 11%), m.p. 89-90 °C. R_f = 0.60 (40:60 ethyl acetate:hexane). δ_H ($CDCl_3$) 1.47 (9H, s, ^tBu), 4.90 (2H, s, CH_2); δ_C ($CDCl_3$, 125MHz) 28.1 (^tBu), 45.2 (CH_2), 84.9 (^tBu), 129.8 (C^5), 145.5 (C^8), 150.6 (C^6), 153.5 (C^2), 153.8 (C^4), 164.4 ($CO_2{}^tBu$); *m/z* (ESMS$^+$) 337.0 (M *(^{35}Cl)* + H, 100%), 339 (M + H, 90%), 341 (M + H, 30%). HRMS (ES$^+$), found: 337.0024 (M + H); $C_{11}H_{12}{}^{35}Cl_3N_4O_2$ requires 337.0020

5.2.2 Catechol Derivatives

3,4-(Dimethyl)methylenedioxyhydrocinnamic acid[3]

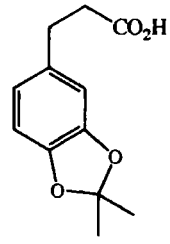

3,4-Dihydroxyhydrocinnamic acid (2.0 g, 11.04 mmol), 2,2-dimethoxypropane (7.0 ml, 55.20 mmol) and *p*-toluene sulphonic acid (35 mg) were dissolved in toluene (60 ml) and boiled under reflux at 160°C, under Soxhlet conditions for 18 hours. The solvent was removed under reduced pressure and the crude reaction mixture was purified via column chromatography (silica, DCM → 10% MeOH:DCM) to yield a yellow solid (510 mg, 2.30 mmol, 21%), m.p. 114-115 °C. R_f = 0.51, 20% MeOH:DCM. δ_H ($CDCl_3$) 1.66 (6H, s, 2 x CH_3), 2.64 (2H, t, *J* 7.8, CH_2CO_2H), 2.86 (2H, t, *J* 7.8, CH_2Ar), 6.62 (3H, m, 3 x benzyl H); δ_C ($CDCl_3$, 125MHz) 26.0 (2 x CH_3), 30.5 (CH_2Ar), 36.2 (CH_2CO_2H), 108.2 (benzyl C), 108.7 (benzyl C), 117.9 (benzyl C), 120.6 ($C(CH_3)_2$), 133.4 (benzyl C), 146.0 (benzyl C), 147.6 (benzyl C), 179.5 (CO_2H); *m/z* (ESMS$^-$) 221 (M - H, 100%).

N-Chloroethanoyl dopamine

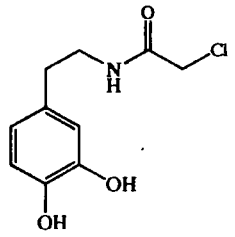

Dopamine (1.0 g, 5.27 mmol) was dissolved in water (10 ml) and chloroacetyl chloride in DCM (10 ml) and the 2 layers were stirred gently for 24 hours, monitoring the pH and adjusting accordingly to 7. The water was evaporated from the aqueous layer yielding a crude brown solid. On the addition of DCM and then MeOH, a white solid precipitated out of solution. The organic soluble fractions were purified via column chromatography (silica, 3% MeOH:DCM → 15% MeOH:DCM; R_f = 0.24, 20% MeOH:DCM) yielding a pale yellow oil.

The white solid was the mono-O-chloroethanoyl ester (220 mg, 0.96 mmol, 18%). δ_H (D_2O) 3.06 (2H, t, J 7.2, CH_2), 3.41 (2H, t, *J* 7.2, CH_2), 4.24 (2H, s, CH_2Cl), 7.05 (3H, m, 3 x benzyl H); δ_C (D_2O, 125MHz) 32.4 (CH_2Ar), 41.2 (CH_2Cl), 44.5 (CH_2NH_2), 117.0 (benzyl C), 117.1 (benzyl C), 121.8 (benzyl C), 129.8 (benzyl C), 143.2 (benzyl C), 144.4 (benzyl C), 176.0 (O-C=O); *m/z* ($ESMS^+$) 252 (M + Na, 100%).

The yellow oil was the desired isomeric amide (130 mg, 0.57 mmol, 19%). δ_H (D_2O) 2.69 (2H, t, *J* 7.6, CH_2), 3.41 (2H, t, *J* 7..6, CH_2), 4.01 (2H, s, CH_2Cl), 6.77 (3H, m, 3 x benzyl H); δ_C (D_2O, 125MHz) 33.7 (CH_2Ar), 41.2 (CH_2Cl), 49.0 (CH_2NHCO), 116.3 (benzyl C), 116.8 (benzyl C), 121.3 (benzyl C), 131.9 (benzyl C), 142.5 (benzyl C), 143.9 (benzyl C), 169.6 (C=O); *m/z* ($ESMS^+$) 252 (M + Na, 100%).

N-Chloroethanoyl-3,4-methylenedioxybenzylamine

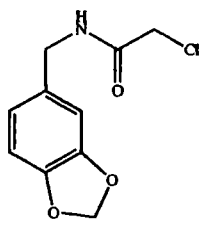

3,4-Methylenedioxybenzylamine (0.13 ml, 1.04 mmol) and 1-(2-chloroacetyl)pyrrolidine-2,5-dione (200 mg, 1.04 mmol) were dissolved in dry

triethylamine (0.18 ml, 1.25 mmol) and THF (5 ml) and the solution was stirred at room temperature for 2 hours. The thick white precipitate formed was filtered and the solid washed with THF. The solvent was then removed yielding a yellow oil which was taken into methanol to give a yellow solid. The solid was washed with various aqueous washes (pH 2, 7, 9) and dried (K_2CO_3) yielding the title compound as a pale yellow solid (170 mg, 0.75 mmol, 72%), m.p. 113-114 °C. R_f = 0.75 (5% MeOH:DCM). δ_H ($CDCl_3$) 4.09 (2H, s, CH_2Cl), 4.39 (2H, d, *J* 6.0, CH_2NH), 5.95 (2H, s, OCH_2O), 6.77 (3H, m, 3 x benzyl H); δ_C ($CDCl_3$, 125MHz) 42.7 (CH_2Cl), 43.8 (CH_2NH), 101.3 (OCH_2O), 108.5 (benzyl C), 108.6 (benzyl C), 121.4 (benzyl C), 131.2 (benzyl C), 147.4 (benzyl C), 148.1 (benzyl C), 165.8 (C=O); *m/z* ($ESMS^+$) 228 (M + H, 15%), 250 (M + Na, 100%).

5.2.3 Ligand and Complex

1,7-(Benzyloxycarbonyl)-1,4,7,10-tetraazacyclododecane[4]

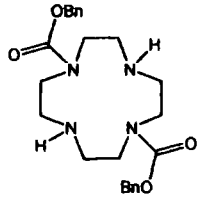

Cyclen (5.0 g, 29.02 mmol) and disodium hydrogen phosphate (14.0 g, 98.62 mmol) were dissolved in purite water (50 ml) and dioxane (20 ml), and the pH adjusted to 2.5 by addition of conc. HCl. A solution of benzyl chloroformate (10.0 ml, 70.05 mmol) and dioxane (10 ml) was added to the solution over 3 hours at room temperature. The solution was stirred at room temperature for 18 hours to yield a thick white solution. Dioxane was removed under reduced pressure and the pH of the aqueous solution adjusted to 7 via the addition of conc. KOH. The solution was extracted with diethyl ether (3 x 50 ml) to remove side products, and the aqueous phase then extracted with DCM (3 x 50 ml). The organic phase was dried with $MgSO_4$ and the solvent was removed under reduced pressure to yield the product as a colourless oil. Diethyl ether (3 x 50 ml) was added to the oil and removed under reduced pressure to yield a white solid (5.2 g, 11.82 mmol, 41%), m.p. 113-116 °C (lit. 115-116 °C). δ_H ($CDCl_3$) 2.85 (8H, m br, 4 x cyclen CH_2), 3.53 (8H, m br, 4 x cyclen CH_2), 5.01 (4H, s, 2 x benzyl CH_2), 7.18

(10H, m, 2 x benzyl); δ_C ($CDCl_3$, 100 MHz) 48.6-49.3 (cyclen CH_2), 67.2 (benzyl CH_2), 127.4-128.2 (benzyl CH), 135.5 (benzyl C), 155.5 (2 x CO_2Bn); *m/z* ($ESMS^+$) 441.2 (M + H, 100%), 917.5 (2M + 2H + Cl, 60%).

1,7–bis(Benzyloxycarbonyl)–4,10–bis(tert-butoxycarbonylmethyl)–1,4,7,10–tetraazacyclododecane

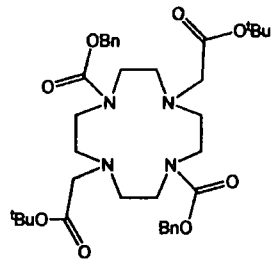

1,7–(Benzyloxycarbonyl)–1,4,7,10-tetraazacyclododecane (1.85 g, 4.20 mmol), K_2CO_3 (1.52 g, 0.011 mol), KI and *tert*-butylbromoacetate (1.48 ml, 0.010 mol) were dissolved in dry acetonitrile (15ml) and the clear solution refluxed overnight. The yellow reaction mixture was then allowed to cool and the solvent removed under reduced pressure. The crude yellow oil was then taken into DCM and the salts removed via filtration. A column was ran to remove the quaternary salt (silica, DCM → 0.5 MeOH:DCM) and the product was collected as a yellow oil (850 mg, 1.27 mmol, 30%). δ_H ($CDCl_3$) 1.42 (18H, s, 2 x ^{t}Bu), 2.86-3.41 (20H, m br, 8 x cyclen CH_2 and 2 x CH_2), 5.12 (4H, s, 2 x benzyl CH_2), 7.33 (10H, m, 2 x benzyl); δ_C ($CDCl_3$, 125MHz) 28.3 (^{t}Bu CH_3), 46.8 (cyclen), 54.2 (cyclen), 56.1 (CH_2), 67.1 (benzyl CH_2), 81.1 (^{t}Bu C), 128.6 (benzyl CH), 137.1 (benzyl C), 156.6 (CO_2Bn), 170.7 ($CO_2{}^t$Bu); *m/z* ($ESMS^+$) 669 (M + H, 100%), 691 (M + Na, 15%). HRMS (ES^+), found: 669.3869 (M + H); $C_{36}H_{53}N_4O_8$ requires 669.3858

1,7–bis(tert-Butoxycarbonylmethyl)–1,4,7,10-tetraazacyclododecane

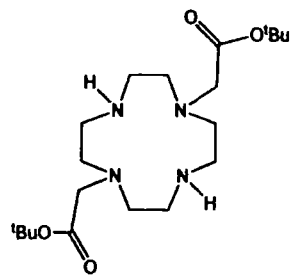

1,7–bis(Benzyloxycarbonyl)–4,10–bis(tert-butoxycarbonylmethyl)–1,4,7,10–tetraazacyclododecane (430 mg, 0.82 mmol) was dissolved in methanol and about 10 mgs of palladium hydroxide on carbon was added. The reaction mixture was then hydrogenated at room temperature under 1 atm H_2. The solution was filtered to remove catalyst, and solvent removed under reduced pressure to yield a pale yellow solid (244 mg, 0.96 mmol, 86%). δ_H ($CDCl_3$) 1.45 (18H, s, 2 x ^tBu), 2.84-3.41 (16H, m, 8 x cyclen CH_2), 3.48 (2H, s, 2 x CH_2); δ_C ($CDCl_3$, 100MHz) 28.3 (^tBu CH_3), 47.3 (cyclen), 51.9 (cyclen), 56.9 (CH_2), 81.5 (^tBu C), 171.2 (C=O); *m/z* (ESMS$^+$) 401 (M + H, 100%). HRMS (ES$^+$), found: 401.3126 (M + H); $C_{20}H_{41}N_4O_4$ requires 401.3122

1-(3-Methyl-10,11,12,13-tetrahydrodipyrido-[3,2-a:2',3'-c]-phenazine)-4,10–bis(tert-butoxycarbonylmethyl)–1,4,7,10-tetraazacyclododecane

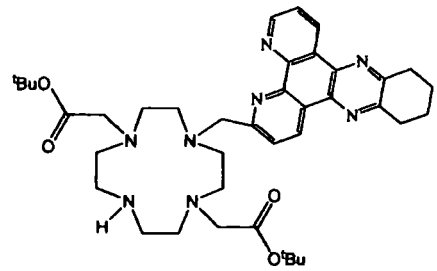

1,7–bis(tert-Butoxycarbonylmethyl)–1,4,7,10-tetraazacyclododecane (150 mg, 0.37 mmol) and $NaHCO_3$ (31 mg, 0.37 mmol) and 3-chloromethyl-10,11,12,13-tetrahydrodipyrido[3,2-a:2',3'-c]phenazine (125 mg, 0.37 mmol) were stirred in dry acetonitrile (5 ml) at 70°C for 100 hours under argon, monitoring progress of the reaction by NMR. The reaction mixture was then filtered and the solvent removed under reduced pressure. Column chromatography (Silica, DCM → 5% MeOH:DCM, R_f=0.20, 5% MeOH:DCM) yielded a pale yellow oil (170 mg, 0.64 mmol, 53%). δ_H ($CDCl_3$) 1.36 (18H, s, 2 x ^tBu), 2.09 (4H, m, H^{10}, H^{13}), 2.68-3.06 (16H, m br, 8 x cyclen CH_2), 3.24 (4H, m, H^{11}, H^{12}), 3.63 (4H, m, 4 x $CH_2CO_2{}^tBu$), 4.08 (2H, s, CH_2dpqC), 7.76 (1H, d, *J* 8.0, H^2), 7.90 (1H, dd, *J* 4.4, 8.0, H^7), 9.43 (1H, d, *J* 8.0, H^1), 9.51 (1H, dd, *J* 1.6, 8.0, H^8), 9.81 (1H, dd, *J* 1.6, 4.4, H^6); *m/z* (ESMS$^+$) 669 (M + H, 100%). HRMS (ES$^+$), found: 699.4338 (M + H); $C_{39}H_{55}N_8O_4$ requires 699.4341

1-(3-Methyl-10,11,12,13-tetrahydrodipyrido[3,2-a:2',3'-c]phenazine)-7-(ethanoyl-3,4-methylenedioxybenzylamine)-4,10–bis(tert-butoxycarbonylmethyl)–1,4,7,10-tetraazacyclododecane

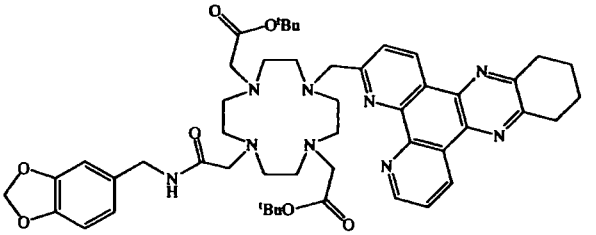

1-(3-Methyl-10,11,12,13-tetrahydrodipyrido[3,2-a:2',3'-c]phenazine)-4,10–bis(tert-butoxycarbonylmethyl)–1,4,7,10-tetraazacyclododecane (25 mg, 0.036 mmol) was dissolved in dry acetonitrile (5 ml) with Cs_2CO_3 (20 mg, 0.057 mmol) and N-chloroethanoyl-3,4-methylenedioxybenzylamine (8 mg, 0.036 mmol) and the mixture was heated at 70°C (bath temperature) under argon conditions for 100 hours. The solvent was removed and the crude oil taken into chloroform and washed with water (pH 7, 9), and dried with K_2CO_3; removal of solvent yielded a pale brown oil (26 mg, 0.029 mmol, 81%). δ_H ($CDCl_3$) 1.43 (18H, s, 2 x ^tBu), 2.09 (4H, m, H^{10}, H^{13}), 2.68-3.06 (16H, m br, 8 x cyclen CH_2), 3.24 (4H, m, H^{11}, H^{12}), 3.63 (4H, m, 2 x $CH_2CO_2{}^tBu$), 4.08 (2H, s, CH_2dpqC), 4.38 (2H, d, *J* 5.6, CH_2NH), 4.59 (2H, s, O=C-CH_2), 5.29 (2H, s, OCH_2O), 5.86-5.93 (3H, m, 3 x benzyl H), 7.72 (1H, dd, *J* 8.4, 4.0, H^7), 8.14 (1H, d, *J* 8.0, H^2), 9.24 (1H, dd, *J* 3.2, 0.8, H^6), 9.33 (1H, d, *J* 8.0, H^1), 9.45 (1H, dd, *J* 8.4, 0.8 H^8).

1-(3-Methyl-10,11,12,13-tetrahydrodipyrido[3,2-a:2',3'-c]phenazine)-7-(ethanoyl-3,4-methylenedioxybenzylamine)-4,10–bis(carboxymethyl)–1,4,7,10-tetraazacyclododecane

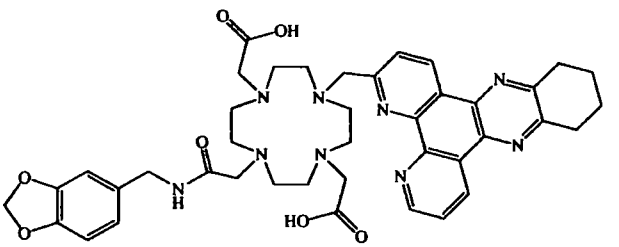

1-(3-Methyl-10,11,12,13-tetrahydrodipyrido[3,2-a:2',3'-c]phenazine)-7-(ethanoyl-3,4-methylenedioxybenzylamine)-4,10–bis(tert-butoxycarbonylmethyl)–1,4,7,10-tetraazacyclododecane (25 mg, 0.028 mmol) was stirred in TFA:DCM, 1:1 for 18 hours. The solvents were removed and the crude product washed with DCM (3 x 5 cm^3) under reduced pressure to yield the bis trifluoroacetate salt of the title compound as a brown oil (20 mg, 0.026 mmol, 92%). δ_H ($CDCl_3$) 2.14 (4H, m, H10, H13), 3.29-3.75 (24H, m

br, 8 x cyclen CH_2, H11, H12, 2 x CH_2CO_2H, CH_2dpqC), 4.40 (2H, d, *J* 5.6, CH_2NH), 5.49 (2H, s, O=C-CH_2), 5.91 (2H, s, OCH_2O), 6.82-6.88 (3H, m, 3 x benzyl H), 8.30 (1H, dd, *J* 8.0, 5.4, H^7), 8.41 (1H, d, *J* 8.4, H^2), 9.30 (1H, dd, *J* 5.4, 0.8, H^6), 9.41 (1H, d, *J* 8.4, H^1), 9.98 (1H, dd, *J* 8.0, 0.8, H^8).

[Eu.Q1]$^+$

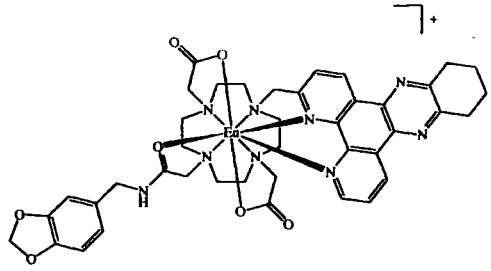

1-(3-Methyl-10,11,12,13-tetrahydrodipyrido[3,2-a:2',3'-c]phenazine)-7-(ethanoyl-3,4-methylenedioxybenzylamine)-4,10–bis(carboxymethyl)–1,4,7,10-tetraazacyclododecane (10 mg, 0.013 mmol) and $EuCl_3.3H_2O$ (4.7 mg, 0.013 mmol) were dissolved in MeOH:H_2O (1:1, 3cm^3). The pH of the solution was adjusted to 5.5 by addition of aqueous KOH, and the reaction mixture heated to 90°C for 24 hours. The pH of the solution was adjusted to 10, by the addition of dilute aqueous KOH solution. The fine precipitate was removed via centrifuging the solution and the water removed under reduced pressure. The pH of the white solid was re-adjusted to pH 7 and the solution filtered via syringe filtration. Water was again removed under reduced pressure, yielding the crude complex as a white solid (10 mg, 0.011 mmol, 83%), m.p. > 250°C. *m/z* (ESMS$^+$) 928 (M^+, 100%), 926 (M^+, 40%), 929 (M^+, 30%). HRMS (ES$^+$), found: 928.2697 (M^+); $EuC_{41}H_{45}N_9O_7^+$ requires 928.2649; λ_{ex} (H_2O): 348 nm; τ_{H2O}: 0.69 ms; τ_{D2O}: 1.01 ms; ϕ_{H2O}: 0.049; t_R (HPLC): 8.35 min (see section 3.2.3 for discussion of these values).

[Tb.Q1]$^+$

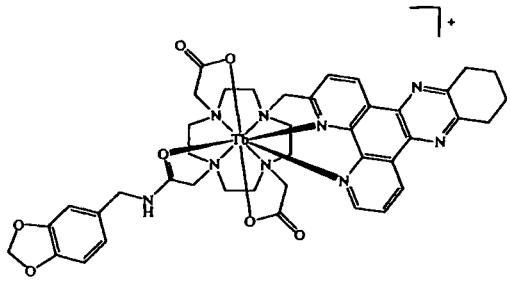

1-(3-Methyl-10,11,12,13-tetrahydrodipyrido[3,2-a:2',3'-c]phenazine)-7-(ethanoyl-3,4-methylenedioxybenzylamine)-4,10-(carboxymethyl)-1,4,7,10-tetraazacyclododecane (10 mg, 0.013 mmol) and $TbCl_3.3H_2O$ (4.9 mg, 0.013 mmol) were dissolved in MeOH:H_2O (1:1, 3cm^3). The pH of the solution was adjusted to 5.5 by addition of aqueous KOH, and the reaction mixture heated to 90°C for 24 hours. The pH of the solution was adjusted to 10, by the addition of dilute aqueous KOH solution. The fine precipitate was removed via centrifuging the solution and the water removed under reduced pressure. The pH of the white solid was re-adjusted to pH 7 and the solution filtered via syringe filtration. Water was again removed under reduced pressure, yielding the crude complex as a white solid (5 mg, 0.005 mmol, 38%), m.p. > 250°C. A sample of this complex was purified by preparative HPLC (Phenomenex Synergi 4μ Fusion-RP 80 column; H_2O + 0.1% formic acid / CH_3CN + 0.1% formic acid). *m/z* (ESMS$^+$) 934 (M^+, 100%), 935 (M^+, 45%), 936 (M^+, 10%), 937 (M^+, 5%). HRMS (ES$^+$), found: 934.2697 (M^+); $TbC_{41}H_{45}N_9O_7^+$ requires 934.2690; λ_{ex} (H_2O): 348 nm; τ_{H2O}: 0.47 ms; τ_{D2O}: 0.69 ms; t_R (HPLC): 8.30 min (see section 3.2.3 for discussion of these values).

References

[1] J. Davoll and B. A. Lowy, *J. Am. Chem. Soc.*, 1951, **73**, 2936

[2] E. Fischer, *Ber.*, 1897, **30**, 2220

[3] T. W. Greene and P. G. M. Wuts, in *Protective Groups in Organic Synthesis*, John Wiley & Sons Ltd., 1999, 3rd Ed., p.287

[4] Z. Kovacs and A. D. Sherry, *J. Chem Soc., Chem. Commun.*, 1995, 185